```
Protein      position                              Amino acid sequence                                                                              position
PyRhopH1AP   245   YGIGIYNQIGSHYIALGHFITLKMAFKHFNKYFV-NGDLKFYTWGMILQFTPEDRFKALDLICDD-TYPKKNKINKKNTIIKSRITGSSQD----------CSVLEFLIHQYNIY--QIEL   351
PfClag9      245   YHIGIFNMIGSHYIAVGHFITLKLALKNYKKYFE-IGSLKYLNWQSILKFNQSDRFKVLDLICDE-SSWYEGQMKRREQYLKNNIFSTSEE----------CSVLEFLIHHMNKY--QMEL   351
PvRhopH1     251   FGIAMYNIVGSNLVALGHFVVLQLALKKYDQFFK-FGKMRFFNWQKILSFSATDRFRVLDAMCNV-QGVQDVQTKRRIVYLKSDRTASFDE----------CNILEFLVHHFNKY--QNSL   361
PyRhopH1A    233   HRIGLFHLIGPHFPALGHFITLSLALKNYENFFE-KGKGHFISWQKLLSFNMSDRFKALDLMCNV-EGTYDIKKKRRITYLEQNRKGAFDE----------CNILEFLIHYFNKY--QLSL   343
PfClag2      294   YGLGLINDLGPHLIALGHFMVLKLALKNYKNYFE-AKNTKFFSWQKILEFSLTDRFKILDMMCDH-DVVYYSQDKRRKTYLNVDTSGSSME----------CNILEFLIHYFNKY--QLEI   400
PkRON2      1055   LNYEIYIAASSNIYLLGHLLMLSLAYLSYNHYFV-QGLKHFYSLETMLMANSDYTFFMYNEVCNV-YYQPKKLFDKDITFIPIESRPGRHSTYVGERKVTCDLLELILNAYTLI--NIHE  1174
PvRON2      1115   LNYEIYIASSSNIYLMGHLLMLSLAYLSYNSYFV-QGLKPFYSLETMLMANSDYSFFMYNEVCNV-YYHPKGTFNKDITFIPIESRPGRHSTYVGERKVTCDLLELILNAYTLI--NVHE  1234
PyRON2      1127   LNYEIYIVSSSNIYLFGHMLLLSLAYLSYNSYFT-KGTKSFYSMETMLLANSDYSFFMYNEMCNV-YYRXNKSFKKDLTFIPIELRPGRYTTYVGERKIICNTLELILNAISLI--NINE  1246
PbRON2       992   LNYEIYIVSSSNIYLFGHMLLLSLAYLSYNSYFT-KGTKSFYSMETMLLANSDYSFFMYNEMCNV-YYRPNKSFKKDLTFIPIELRPGRYTTYVGERKIICDTLELILNAVSLI--NINE  1111
PchRON2      909   LNYEIYILSSSNIYLFGHMLLLSLAYLSYNSYFT-KGTKSFYSMETLLLANSDYSFFMLNEMCNV-YYKPNKSFKKDLTFIPIELRPGRYSTYVGERRILCDTLELILNAVSLI--NINE  1028
PfRON2      1105   FNYEIHMASASNIYLLAHFLVLSLAYLSYNEYFT-TGTKSFYSLPTILTANSDNSFFMLNEMCNI-HYNPNKNFKKDITFIPIESRPKRTTTFYGERRLTCDLLELVLNAIMLI--NINE  1224
TaRON2       422   LGADMFWVSGNNPFILGHLATMMLGYTEYESFFSDYPKRRFYSWLELVRSGPGGSINRLDYMCGVRRGSRYARGSNGLVYKKISTAKRYEHNVSSDGVFLCEMLEVLLRSINLTMDSMGD   541
TpRON2       424   LGADMFWVSGNNPFILGHLATMMLGYTEYESFFSDYPKRRFYSWLELVRSGPGGSVNRLDYMCGIRRGSRYARGSNGLVYKKISTAKRYEHNVSSDGVFLCEMLEVLLRSINLTMDSMGD   543
BbigRON2     343   LGMELFAACGNNPFLLGHLATNMLAYTQYKLFFDGDQGRPFYTWLDLVKSG---NLDMLDRMCGTIRGPKYKRDSNGAVTVNKNRKRKDDPQLNADGVFLCNLLEVLLVSIDASIDAMGQ   459

                   TM predicted by TMpred
                   <======== region identified by BLASTP search ========

PyRhopH1AP   352   FKKASILN----LNMQLFLDTDSLKQNFFNFMCKKNNE-------CNIYKGPHFKQE    397
PfClag9      352   YSKMHKLS----LNVQIYLENKHLKEKFLQFMCRSRKE-------CNIYESDRFKQE    397
PvRhopH1     362   VSGLYQED----FKTHYLQEHSDIRNEFFKFMCNDINH-------CNIYSSKLFLSE    403
PyRhopH1A    344   ISRTYGDE----FQSYYLLEHKDMKEEFFRFMCDSSKN-------CNIYNSSIFLSN    358
PfClag2      401   IKATQDTD----FELHGMMEHKNIKDYFFSFMCNDPKE-------CIIYHTNQFKKE    446
PkRON2      1175   IQKVFNNSDTYGYENSISFAHNAVR--IFSQVCPRDDAKNT-LSCDFEKSTLYNPK   1223
PvRON2      1235   IQKVFNTSEAYGYENSISFGHNAVR--IFSQVCPRDDAKNT-FGCDFEKSTLYNSK   1283
PyRON2      1247   IYNVFHKNNVYGYENSVSFSNNAIR--VFSQVCPRNMEKNI-INCSFEKSTLYKAN   1295
PbRON2      1112   VYNVFHKNNVYGYENSVSFSNNAIR--VFSQVCPRNMEKNI-INCSFEKSTLYKGN   1160
PchRON2     1029   IYNVFYKNNVNGYENSVSFSNNAIR--IFSQVCPRRNEKNT-ISCSFEDSNLYKKV   1077
PfRON2      1225   INNVFSNNNVDGYENSLSFSHNAIR--IFSKVCPKINNDNV-LKCEFEESSLYNPK   1273
TaRON2       542   LLNQKGGN----YEPNVGSIINGKR--MQAKLCSNPGDGTIAVRCDFEHSRLLGEE    591
TpRON2       544   LLNQKGGS----YEPNVGSIINGKR--MQAKLCSNPGDGTIAVRCDFEHSVLVGEE    593
BbigRON2     460   LLSQYGVP----YEHSVGAIANGRR--MQAFVCSDPRESAIVVRCDFMSSTLNSSK    509

                   ========================================>
```

Fig. 2. Amino acid alignment of *Plasmodium* RON2 and RhopH1/Clag. Alignment was generated by MUSCLE [24] with manual correction. "*" indicates that the residues in that column are identical in all sequences in the alignment. ":" indicates conserved substitutions and "." indicates semi-conserved substitutions. In addition to 9 RON2 sequences, *P. falciparum* Clag2 (AAC71977), Clag9 (CAD52032), *P. yoelii* RhopH1A (BAB70675), RhopH1AP (BAB70677), and *Pv*RhopH1 (contig 1047) were used to generate the alignment. Cys residues are highlighted in red. The region possessing homology between RhopH1/Clag and RON2 as identified by BLASTP is indicated by the bar under the alignment.

residues in the cytoplasmic loops of the transmembrane protein [21], which is a likely explanation for this discrepancy.

3.3. *Pf*RON2 transcription peaks at the schizont stage

To determine the transcription pattern in the asexual stages of the parasite life-cycle, quantitative RT-PCR was performed on the HB3 parasite line prepared from a synchronized culture harvested at 6 h intervals. Both RON2 and AMA1 transcriptions were seen to peak around 36–40 h after invasion, when parasites were in the schizont stage. AMA1 showed a broader and flatter transcription peak than RON2 (Fig. 3). Transcriptome data compiled in the PlasmoDB website [13,29] also indicated a milder wave crest of AMA1 transcripts compared with RON2.

3.4. Complex formation of *Pf*RON2, *Pf*RON4, and *Pf*AMA1

Mouse and rabbit anti-*Pf*RON2 sera were generated using recombinant GST-fRON2N. Firstly, we evaluated the reactivity of anti-*Pf*RON2 sera by Western blot using recombinant proteins. Both antisera recognized the fRON2N component of the recombinant protein after cleavage (Fig. S3, filled arrows). Cleaved 26.4-kDa GST component (Fig. S3, arrowheads) and 46-kDa GST-fused PreScission protease (Fig. S3, unfilled arrow) were also recognized by these Abs.

Secondly, we evaluated the reactivity of these sera against native RON2 proteins extracted from schizont stage *P. falciparum* (HB3 line) by Western blot analysis. Both antisera reacted with a band slightly larger than 250 kDa (Fig. 4A, arrows), which is similar to the predicted molecular weight of *Pf*RON2 after exclusion of the putative signal peptide sequence (247 kDa). An 80-kDa band was detected by both mouse and rabbit antisera in HB3 extract, for which the exact identity is not known, but a possible processed product of *Pf*RON2. A 55-kDa band detected with rabbit antiserum was also detected with preimmune serum, suggesting that this band was unrelated to

Fig. 3. Transcriptional analysis by quantitative RT-PCR of *pfrhoph2*, *pfron2*, and *pfama1* genes during blood stages of *P. falciparum* (HB3 line). Y-axis indicates copy number of each transcript detected per 1000 parasites. Similar results were observed in 3 independent experiments (data not shown).

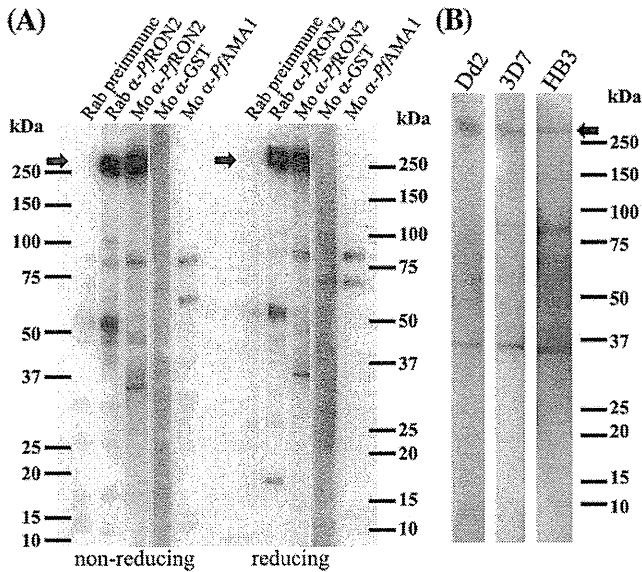

Fig. 4. Western blot analysis of antisera against native parasite proteins. (A) Schizont-enriched parasite extracts were stained by rabbit preimmune serum, (Rab preimmune), rabbit anti-*Pf*RON2 (Rab α-*Pf*RON2), mouse anti-fRON2N (Mo α-*Pf*RON2), and Abs against GST (Mo α-GST) or *Pf*AMA1 (Mo α-*Pf*AMA1) under both reducing and non-reducing conditions. Both mouse and rabbit anti-*Pf*RON2 sera detected a band slightly larger than 250 kDa. (B) Western blot of schizont-enriched parasite extracts from 3 different *P. falciparum* lines, Dd2, 3D7, and HB3 with mouse anti-fRON2N serum. Arrows indicate predicted *Pf*RON2 bands.

*Pf*RON2. A 35-kDa band was detected with mouse antiserum but not with rabbit antiserum, suggesting that it is also unrelated to RON2.

To evaluate the interaction between *Pf*RON2, *Pf*RON4, and *Pf*AMA1, we performed immunoblotting against immunoprecipitated materials from mature schizont-rich parasite extracts (Fig. 5). We found that RON2 was detected in the precipitated fraction using anti-*Pf*AMA1 or anti-*Pf*RON4. In the reciprocal experiment, *Pf*AMA1 and *Pf*RON4 were also detected in the precipitated fraction of anti-*Pf*RON2 serum. Although it is theoretically possible that such immunoprecipitated fractions contained the *Pf*RON2-*Pf*RON4, *Pf*RON2-*Pf*AMA1, and *Pf*RON4-*Pf*AMA1 dimeric complexes as appropriate to the primary

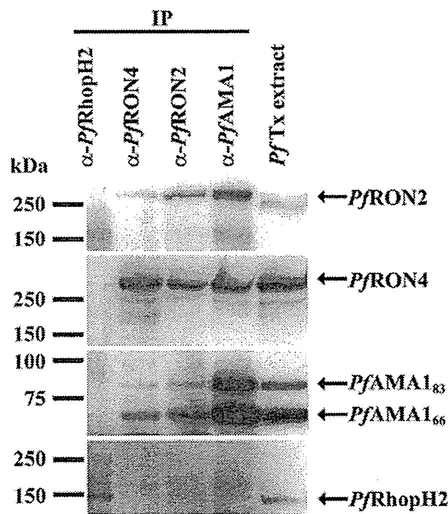

Fig. 5. *Pf*RON2 is co-precipitated with *Pf*RON4 and *Pf*AMA1. Schizont-rich parasite Triton X-100 extracts (*Pf* Tx extract) were immunoprecipitated (IP) with rabbit sera against *Pf*RhopH2 (α-*Pf*RhopH2), *Pf*RON2 (α-*Pf*RON2), *Pf*AMA1 (α-*Pf*AMA1) or mouse monoclonal Ab against *Pf*RON4 (α-*Pf*RON4), then stained against *Pf*RON2, *Pf*AMA1, *Pf*RON4, or *Pf*RhopH2. $AMA1_{83}$ is a proprotein form and $AMA1_{66}$ is a processed form.

antibody, considering that these 3 proteins are distinct molecules that do not possess any similarity each other, this specific co-immunoprecipitation suggests complex formation among *Pf*RON2, *Pf*RON4, and *Pf*AMA1 in *P. falciparum*. The fact that both the 83-kDa proform and the 66-kDa processed form were co-precipitated with *Pf*RON2 indicated that a region responsible for complex formation was located in the 66-kDa form of AMA1 [30]. Neither of these was detected in the anti-RhopH2 immunoprecipitate, thereby excluding not only the possibility of *Pf*RON2 involvement in the RhopH complex, but also potential carryover due to insufficient or inadequate washing steps.

3.5. RON2 is expressed at the rhoptry neck of Plasmodium merozoites

Dual labeling indirect immunofluorescent assay was performed using anti-*Pf*RON2 with either anti-*Pf*AMA1 (microneme marker), anti-Clag3.1 (rhoptry body marker), or anti-*Pf*RON4 (rhoptry neck marker) antibodies in order to determine the sub-cellular location of *Pf*RON2 in *P. falciparum* (Fig. 6). In segmented schizonts, RON2 antisera produced a punctate pattern of fluorescence and each developing merozoite showed a single small punctate *Pf*RON2-positive signal located at the apical end. Although some parts of the *Pf*RON2 signal

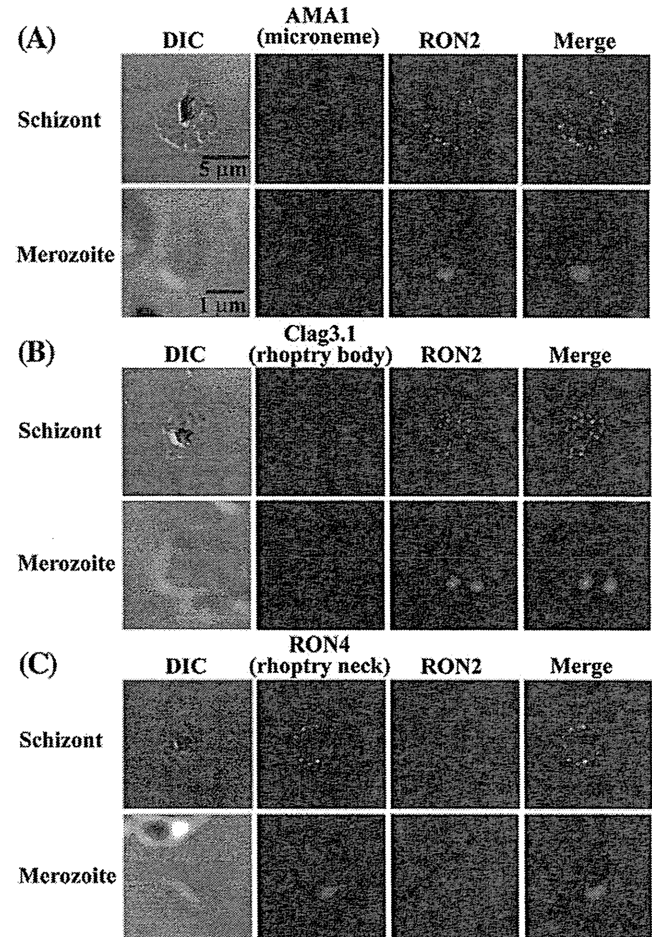

Fig. 6. *Pf*RON2 is expressed at the apical end of *Plasmodium* merozoites. Schizont-infected erythrocytes and merozoites were dual-labeled with antisera against *Pf*RON2 and *Pf*AMA1 (A), *Pf*Clag3.1 (B), or *Pf*RON4 (C). Merged images are shown in the right panels. All segmented schizonts and merozoites are positive for *Pf*RON2. Nuclei are counterstained with DAPI. Colocalization of *Pf*RON2 with *Pf*RON4 (rhoptry neck marker) was observed but neither colocalized with *Pf*Clag3.1 (rhoptry body marker) nor *Pf*AMA1 (microneme marker). To eliminate the background staining, negative control sera were always used and images were assessed (data not shown).

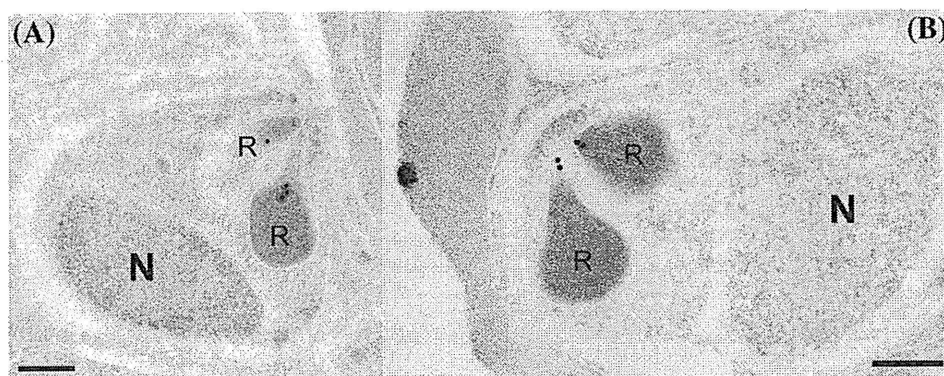

Fig. 7. Rhoptry neck localization of *Pf*RON2 by immunoelectron microscopy. Longitudinally sectioned merozoites in schizont-infected erythrocytes were labeled with anti-*Pf*RON2 serum followed by secondary Ab conjugated with gold particles. Gold particles were restricted to the narrow neck portion of the rhoptries (R). Two different images are shown (A and B). N indicates nucleus. Bars=200 nm.

overlapped with microneme protein AMA1 and rhoptry body protein Clag3.1, it did not colocalize well with those markers, whereas complete colocalization was observed with the rhoptry neck marker *Pf*RON4.

Immunoelectron microscopy was carried out to determine the precise localization of the protein. *Pf*RON2 was detected in the neck portion of the pear-shaped rhoptries in segmented schizonts (Fig. 7). Thus *Pf*RON2 is seen to compartmentalize in the rhoptry neck.

3.6. Potential positive diversifying selection on PfRON2

To evaluate the polymorphic nature of *Pf*RON2, we sequenced the *pfron2* nucleotide sequence (2459–6570), excluding the 5′ low complexity region, in 5 *P. falciparum* parasite lines and compared them with the sequence from the genome database (3D7 line). A total of 5 nonsynonymous nucleotide substitutions were observed at nucleotide positions 2615, 2710, 2914, 4391 and 4392, resulting 4 amino acid substitutions (Table 1). An excess of nonsynonymous substitutions (d_N=0.0007±0.0003) over synonymous substitutions (d_S=0.0002±0.0002) was detected (P=0.0333), indicating *Pf*RON2 is subject to positive diversifying selection.

4. Discussion

In this study, we characterized *P. falciparum* RON2 for its protein structure, transcription profiles, intracellular localization, and complex formation with *Pf*RON4 and *Pf*AMA1.

*Pf*RON2 possesses a region harboring homology with another rhoptry protein RhopH1/Clag, a component of the RhopH complex that possesses erythrocyte binding ability [16,31,32]. Co-immunoprecipitation showed that *Pf*RON2 does not form a complex with RhopH2, suggesting that *Pf*RON2 is unlikely to be a component of the RhopH complex. Because RON2 orthologs can be found in other apicomplexan parasites and RhopH1/Clag is found only in *Plasmodium* species, RhopH1/Clag probably evolved via acquisition of a conserved functional domain from RON2 during its generation in *Plasmodium* species. Thus, this homologous region may have a common function between these two complexes. The sequence of *Tg*RON2 deposited to the database (GenBank accession number DQ096563) only possesses the C-terminal half of the conserved region between RON2 and RhopH1/Clag. By comparing *Tg*RON2 gDNA and cDNA sequences, we noticed that intron 3 is relatively large (2272 bp) and contains a potential sequence encoding the N-terminal portion of the conserved region. Thus it is possible that there is another alternatively spliced transcript encoding the full length of the conserved region. Alternatively, it is also possible that this region represents an ancient vestigial exon.

Interestingly, we could readily detect complex formation between AMA1 and RON proteins in the extract obtained from mature schizont-rich parasites, suggesting that complex formation had already occurred at the schizont stage likely at the apical end upon secretion of RON proteins from rhoptry and AMA1 from microneme. This is in contrast to the other apicomplexa parasite *T. gondii*, in which the AMA1-RON complex was proposed to form at the initial contact with the host cell. The precise timing of the complex formation is not clear, but may vary depending on the parasite species. Among RON proteins characterized thus far, only *Tg*RON4 was visualized to locate at the moving junction during cell invasion. Whether *Pf*RON2 and *Pf*RON4 locate at the moving junction and whether the complex remains intact during cell invasion are still need to be clarified. We found that *Pf*RON2 degraded more rapidly than *Pf*RON4 after extraction (Fig. S4), which may explain the previous observation by Alexander et al. (2006), who did not detect *Pf*RON2 in the immunoprecipitant with anti-*Pf*AMA1 Ab [7].

The association between the 83-kDa proform of *Pf*AMA1 with RON proteins raises the possibility that the processing of *Pf*AMA1 from the 83-kDa form to 66-kDa form occurs not only in the microneme, as previously proposed [33], but also on the apical tip of the merozoite after release from the microneme in mature schizonts. If this is the case, it is not clear whether this AMA1 processing occurs after complex formation with RON proteins or is mainly achieved prior to this. However, it is formally possible that disruption of the different intracellular microorganelles during the experimental procedure resulted in an artificial complex formation of *Pf*AMA1 proform, for which further studies are required.

Due to the fact that *P. falciparum* AMA1 exhibits relatively high polymorphism between lines, which is considered to be generated by positive diversifying selection under the human immune pressure, we evaluated the polymorphic nature of *Pf*RON2. Although the level of polymorphism of RON2 is not high, the fact that $d_N > d_S$ suggests that positive diversifying selection does indeed act on RON2. Three types of

Table 1
Nucleotide and amino acid polymorphism of *Pf*RON2

Nucleotide positions (amino acid) [a]	Parasite line					
	3D7	7G8	HB3	Dd2	FVO	D10
2614–2616	tCa (Ser)	tCa (Ser)	tCa (Ser)	tCa (Ser)	tCa (Ser)	tTa (Leu)
2710–2712	Cat (His)	Cat (His)	Cat (His)	Tat (Tyr)	Tat (Tyr)	Tat (Tyr)
2914–2916	Gac (Asp)	Gac (Asp)	Cac (His)	Gac (Asp)	Gac (Asp)	Gac (Asp)
4390–4392	gAA (Glu)	gAA (Glu)	gAC (Asp)	gGC (Gly)	gGC (Gly)	gAA (Glu)

[a]Nucleotide numbering is after the 3D7 line sequence.

amino acid substitutions found at aa 1464 (Asp, Glu, and Gly) suggests that this particular site is under diversifying selection and is possibly to be exposed to host immunity. Thus, *Pf*RON2 not only appears to have an important role in host cell invasion by apicomplexan parasites, but also is a potential target for malaria intervention strategies.

Acknowledgements

We thank N Iyoku for her expertise, I Ling for anti-*Pf*RhopH2 serum, C Long for anti-*Pf*AMA1 serum, anti-*Pf*RON4 antibody (26C64F12) for J-F Dubremetz, and R Culleton for critical reading. Preliminary sequence data of *P. knowlesi*, *P. berghei*, *P. chabaudi*, and *B. bigemina* were produced by the corresponding groups at the Sanger Institute website at http://www.sanger.ac.uk/. Preliminary sequence data of *P. vivax* was produced at the Institute for Genomic Research website at http://www.tigr.org. This work was supported in part by Grants-in-Aid for Scientific Research 17590372 and 17406009 (to OK) from the Ministry of Education, Culture, Sports, Science and Technology, Japan. JC acknowledges the support of National Natural Science Foundation of China 30700695.

Appendix A. Supplementary data

Supplementary data associated with this article can be found, in the online version, at doi:10.1016/j.parint.2008.09.005.

References

[1] Snow RW, Guerra CA, Noor AM, Myint HY, Hay SI. The global distribution of clinical episodes of *Plasmodium falciparum* malaria. Nature 2005;434:214–7.
[2] Kaneko O. Erythrocyte invasion: vocabulary and grammar of the *Plasmodium* rhoptry. Parasitol Int 2007;56:255–62.
[3] Aikawa M, Miller LH, Johnson J, Rabbege J. Erythrocyte entry by malarial parasites. a moving junction between erythrocyte and parasite. J Cell Biol 1978;77:72–82.
[4] Boothroyd JC, Dubremetz JF. Kiss and spit: the dual roles of *Toxoplasma* rhoptries. Nat Rev Microbiol 2008;6:79–88.
[5] Alexander DL, Mital J, Ward GE, Bradley P, Boothroyd JC. Identification of the moving junction complex of *Toxoplasma gondii*: a collaboration between distinct secretory organelles. PLoS Pathog 2005;1:e17.
[6] Lebrun M, Michelin A, El Hajj H, Poncet J, Bradley PJ, Vial H, et al. The rhoptry neck protein RON4 re-localizes at the moving junction during *Toxoplasma gondii* invasion. Cell Microbiol 2005;7: 1823–33.
[7] Alexander DL, Arastu-Kapur S, Dubremetz JF, Boothroyd JC. *Plasmodium falciparum* AMA1 binds a rhoptry neck protein homologous to TgRON4, a component of the moving junction in *Toxoplasma gondii*. Eukaryot Cell 2006;5:1169–73.
[8] Baum J, Tonkin CJ, Paul AS, Rug M, Smith BJ, Gould SB, et al. A malaria parasite formin regulates actin polymerization and localizes to the parasite-erythrocyte moving junction during invasion. Cell Host Microbe 2008;3:188–98.
[9] Triglia T, Healer J, Caruana SR, Hodder AN, Anders RF, Crabb BS, et al. Apical membrane antigen 1 plays a central role in erythrocyte invasion by *Plasmodium* species. Mol Microbiol 2000;38:706–18.
[10] Hehl AB, Lekutis C, Grigg ME, Bradley PJ, Dubremetz JF, Ortega-Barria E, et al. *Toxoplasma gondii* homologue of *Plasmodium* apical membrane antigen 1 is involved in invasion of host cells. Infect Immun 2000;68:7078–86.
[11] Mital J, Meissner M, Soldati D, Ward GE. Conditional expression of *Toxoplasma gondii* apical membrane antigen-1 (TgAMA1) demonstrates that TgAMA1 plays a critical role in host cell invasion. Mol Biol Cell 2005;16:4341–9.
[12] Trager W, Jensen JB. Human malaria parasites in continuous culture. Science 1976;193:673–5.
[13] Bahl A, Brunk B, Crabtree J, Fraunholz MJ, Gajria B, Grant GR, et al. PlasmoDB: the *Plasmodium* genome resource. a database integrating experimental and computational data. Nucleic Acids Res 2003;31:212–5.
[14] Tsuboi T, Takeo S, Iriko H, Jin L, Tsuchimochi M, Matsuda S, et al. The wheat germ cell-free based production of malaria proteins for discovery of novel vaccine candidates. Infect Immun 2008;76:1702–8.
[15] Ling IT, Kaneko O, Narum DL, Tsuboi T, Howell S, Taylor HM, et al. Characterisation of the *rhoph2* gene of *Plasmodium falciparum* and *Plasmodium yoelii*. Mol Biochem Parasitol 2003;127:47–57.
[16] Kaneko O, Yim Lim BY, Iriko H, Ling IT, Otsuki H, Grainger M, et al. Apical expression of three RhopH1/Clag proteins as components of the *Plasmodium falciparum* RhopH complex. Mol Biochem Parasitol 2005;143:20–8.
[17] Kaneko O, Fidock DA, Schwartz OM, Miller LH. Disruption of the C-terminal region of EBA-175 in the Dd2/Nm clone of *Plasmodium falciparum* does not affect erythrocyte invasion. Mol Biochem Parasitol 2000;110:135–46.
[18] Torii M, Adams JH, Miller LH, Aikawa M. Release of merozoite dense granules during erythrocyte invasion by *Plasmodium knowlesi*. Infect Immun 1989;57: 3230–3.
[19] Aikawa M, Atkinson CT. Immunoelectron microscopy of parasites. Adv Parasitol 1990;29:151–214.
[20] Bendtsen JD, Nielsen H, von Heijne G, Brunak S. Improved prediction of signal peptides: signalP 3.0. J Mol Biol 2004;340:783–95.
[21] Hofmann K, Stoffel W. TMbase — a database of membrane spanning proteins segments. Biol Chem Hoppe-Seyler 1993;374:166.
[22] Krogh A, Larsson B, von Heijne G, Sonnhammer EL. Predicting transmembrane protein topology with a hidden Markov model: application to complete genomes. J Mol Biol 2001;305:567–80.
[23] Linding R, Russell RB, Neduva V, Gibson TJ. GlobPlot: exploring protein sequences for globularity and disorder. Nucleic Acids Res 2003;31:3701–8.
[24] Edgar RC. MUSCLE: multiple sequence alignment with high accuracy and high throughput. Nucleic Acids Res 2004;32:1792–7.
[25] Tamura K, Dudley J, Nei M, Kumar S. MEGA4: Molecular Evolutionary Genetics Analysis (MEGA) software version 4.0. Mol Biol Evol 2007;24:1596–9.
[26] Altschul SF, Madden TL, Schäffer AA, Zhang J, Zhang Z, Miller W, et al. Gapped BLAST and PSI-BLAST: a new generation of protein database search programs. Nucleic Acids Res 1997;25: 3389–402.
[27] Pain A, Renauld H, Berriman M, Murphy L, Yeats CA, Weir W, et al. Genome of the host-cell transforming parasite *Theileria annulata* compared with *T. parva*. Science 2005;309:131–3.
[28] Gardner MJ, Bishop R, Shah T, de Villiers EP, Carlton JM, Hall N, et al. Genome sequence of *Theileria parva*, a bovine pathogen that transforms lymphocytes. Science 2005;309:134–7.
[29] Le Roch KG, Zhou Y, Blair PL, Grainger M, Moch JK, Haynes JD, et al. Discovery of gene function by expression profiling of the malaria parasite life cycle. Science 2003;301:1503–8.
[30] Howell SA, Withers-Martinez C, Kocken CH, Thomas AW, Blackman MJ. Proteolytic processing and primary structure of *Plasmodium falciparum* apical membrane antigen-1. J Biol Chem 2001;276:31311–20.
[31] Ghoneim A, Kaneko O, Tsuboi T, Torii M. The *Plasmodium falciparum* RhopH2 promoter and first 24 amino acids are sufficient to target proteins to the rhoptries. Parasitol Int 2007;56:31–43.
[32] Rungruang T, Kaneko O, Murakami Y, Tsuboi T, Hamamoto H, Akimitsu N, et al. Erythrocyte surface glycosylphosphatidyl inositol anchored receptor for the malaria parasite. Mol Biochem Parasitol 2005;140:13–21.
[33] Healer J, Triglia T, Hodder AN, Gemmill AW, Cowman AF. Functional analysis of *Plasmodium falciparum* apical membrane antigen 1 utilizing interspecies domains. Infect Immun 2005;73:2444–51.

Parasitology International 58 (2009) 101–105

Contents lists available at ScienceDirect

Parasitology International

journal homepage: www.elsevier.com/locate/parint

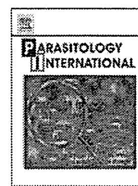

Short communication

Pyruvate kinase type-II isozyme in *Plasmodium falciparum* localizes to the apicoplast

Takuya Maeda [a,1], Tomoya Saito [a], Omar S. Harb [b], David S. Roos [b], Satoru Takeo [c], Hiroko Suzuki [c], Takafumi Tsuboi [c], Tsutomu Takeuchi [a], Takashi Asai [a,*]

[a] *Department of Tropical Medicine and Parasitology, School of Medicine, Keio University, 35 Shinanomachi, Shinjuku-ku, Tokyo 160-8582, Japan*
[b] *Department of Biology, University of Pennsylvania, 301 Goddard Laboratories Philadelphia, PA 19104, USA*
[c] *Cell-Free Science and Technology Research Center, Ehime University, 3 Bunkyo-cho, Matsuyama, Ehime 790-8577, Japan*

ARTICLE INFO

Article history:
Received 16 July 2008
Received in revised form 15 October 2008
Accepted 18 October 2008
Available online 31 October 2008

Keywords:
Plasmodium falciparum
Pyruvate kinase II
Apicoplast
Mitochondria
Cell-free expression

ABSTRACT

Bioinformatics research on *Plasmodium falciparum* revealed two isoforms of pyruvate kinase: type-I and type-II enzymes. The type-I enzyme shows typical glycolytic properties, while type-II enzyme is involved in fatty acid type-II biosynthesis and has been predicted to localize to the apicoplast with the targeting signal in its N-terminus. The type-I and type-II isoforms have the same evolutionary origin as *Toxoplasma gondii* isozymes, *Tg*PyKI and *Tg*PyKII, respectively; however, *Tg*PyKII localizes to both the mitochondrion and the apicoplast. Accordingly, we made a recombinant full length of *P. falciparum* pyruvate kinase type-II protein using a wheat germ cell-free expression system and obtained a specific antibody against the type-II protein. Fluorescent microscopic analysis revealed that *P. falciparum* type-II enzyme was localized only to the apicoplast, not to the mitochondrion. The data suggest differences in localization and metabolic pathways between *P. falciparum* and *T. gondii* pyruvate kinase isoforms.

© 2008 Elsevier Ireland Ltd. All rights reserved.

Pyruvate kinase (EC 2.7.1.40) catalyzes the essentially irreversible transphosphorylation of phosphoenolpyruvate (PEP) to ADP. The activities of most mammalian and bacterial pyruvate kinases are allosterically regulated by fructose 1,6-bisphosphate, and pyruvate kinase is known to play a regulatory role in glycolysis. The glycolytic end product, pyruvate, feeds into various metabolic pathways, and hence pyruvate kinase is important in several primary metabolic reactions.

Many organisms have pyruvate kinase isozymes with different kinetic properties, and most pyruvate kinases in eukaryotes are reported to be located in the cytosol. Two types of pyruvate kinase were characterized in *Toxoplasma gondii* [1,2]. Pyruvate kinase type-II isozyme (*Tg*PyKII) was localized in both the mitochondrion and the apicoplast, whereas pyruvate kinase type-I (*Tg*PyKI) was located in the cytosol. *Tg*PyKII exhibited only 18% overall amino acid identity with *Tg*PyKI and showed novel properties of exhibiting high pH optima and GDP dependency [2].

The malaria bioinformatics website (http://sites.huji.ac.il/malaria/), compiled and maintained by Hagai Ginsburg, reports two isoforms of pyruvate kinase in *Plasmodium falciparum*. The type-I enzyme (*Pf*PyKI) has been characterized enzymologically in detail [3]. The type-II enzyme (*Pf*PyKII) was predicted to have an apicoplast targeting signal in the N-terminus; however, experimental localization has not been confirmed. Phylogenetic analysis indicated that *Pf*PyKI and *Pf*PyKII have the same evolutionary origin as TgPyKI and TgPyKII, respectively, suggesting that type-II has a proteobacterial origin [2]. Thus, we questioned whether both *Pf*PyKII and *Tg*PyKII are localized in both the apicoplasts and the mitochondria.

In this study, we made recombinant *Pf*PyKII protein in a wheat germ cell-free expression system, purified the recombinant protein, created an antibody, and localized *Pf*PyKII by immunofluorescent microscopy.

The *Pf*PyKII gene was amplified from *P. falciparum* genomic DNA. The two primers were 5′-ACTGGATCCCCATATTGCCTATGAT-3′ and 5′-TCGGGATCC CTAATTTGTTAGACATGG-3′ (*Bam*HI site is underlined). The first denaturation at 95 °C was for 10 min and each of 30 reaction cycles consisted of 94 °C for 30 s, 47 °C for 30 s, and 65 °C for 2 min, and a final elongation cycle step at 65 °C for 5 min using KOD-plus DNA polymerase (Toyobo Co. Ltd, Osaka, Japan). Thereafter, the amplified DNA products were treated with *Bam*HI and inserted into a plasmid pEU-E01G-N2 (Cell-Free Science and Technology Research Center, Ehime University, Ehime, Japan) using the LigaFast ligation kit (Promega, Madison, WI, USA) according to the manufacturer's protocol. The plasmid was electroporated into the *Escherichia coli* DH10B (Takara Bio, Kyoto, Japan) and the bacteria were grown in a plate. The right directional clones were detected by DNA sequencing using the ABI PRISM BigDye terminator cycle sequencing kit (Applied Biosystems, Foster, CA, USA) and loaded onto an ABI PRISM 310 DNA sequencer. After plasmid purification

* Corresponding author. Tel.: +81 3 3353 1211x62747; fax: +81 3 3353 5958.
E-mail address: asait@sc.itc.keio.ac.jp (T. Asai).
[1] Present address: International Research Center for Infectious Diseases, The Institute of Medical Science, The University of Tokyo, Shiroganedai 4-6-1, Minato-ku, Tokyo 108-8639, Japan.

1383-5769/$ – see front matter © 2008 Elsevier Ireland Ltd. All rights reserved.
doi:10.1016/j.parint.2008.10.005

using Qiagen Plasmid Midi Kit (Qiagen, Hilden, Germany), the plasmid was further purified by C_5Cl_2 ultra-centrifugation at 391,000 ×g for 16 h at 25 °C to avoid endotoxin contamination. The purified plasmid containing a glutathione S-transferase (GST) coding region and an SP6 promoter upstream of the DNA inserted region was treated with SP6 RNA polymerase (GE Healthcare, Little Chalfont, Buckinghamshire, UK). The method of mRNA production and translation in wheat germ was described previously [4].

The GST-pyruvate kinase isozyme fusion protein in the wheat germ extract was purified using an affinity column of glutathione sepharose 4B (GE Healthcare). The pyruvate kinase isozyme was cut from the fusion protein by PreScission Protease (GE Healthcare) according to

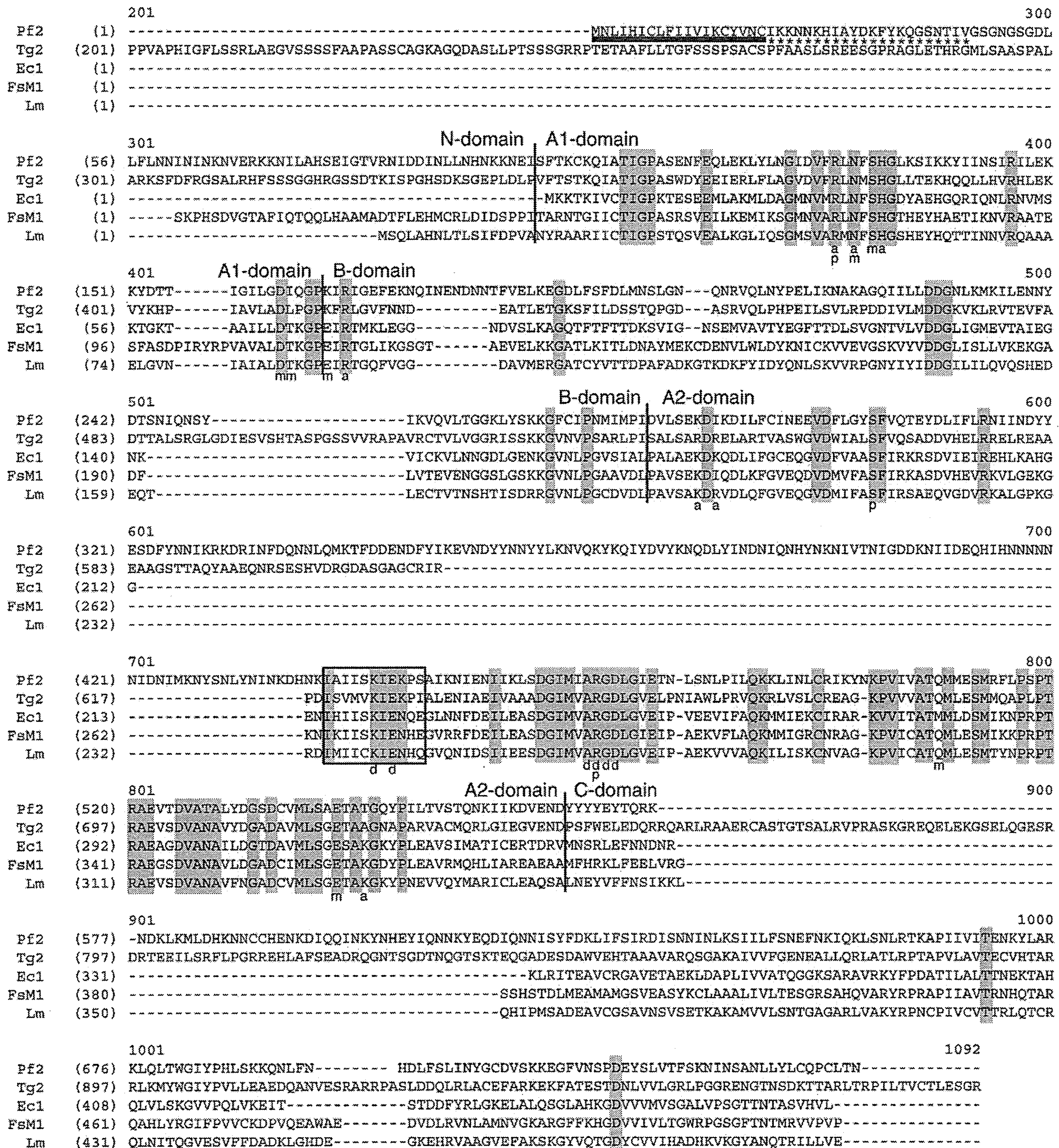

Fig. 1. Amino acid sequence alignment of *P. falciparum* pyruvate kinase type-II isozyme (*Pf*PyKII) with four pyruvate kinases from other species. Sequence data accession numbers are: Pf2, *Pf*PyKII (this study; PF10_0363); Tg2, *Toxoplasma gondii* II (AB118155); Ec1, *Escherichia coli* isozyme I (1PKY_A); FsM1, *Felis catus* isozyme M1 (P11979); Lm, *Leishmania mexicana* (CAA52898). *Vertical lines* indicate divisions between four three-dimensional domains (N, A, B, and C) as described previously [10]. An open black *box* indicates the pyruvate kinase signature sequence (PROSITE, PS00110); *p* indicates PEP binding sites; *a*, ADP binding sites; *d*, divalent cation binding sites; *m*, monovalent cation binding sites; *dashes*, gaps in the alignment. DNA sequences analyses were performed using the VectorNTI suite (InforMax, Executive Way Frederick, MD, USA). The thick underline in the N-terminal of *P. falciparum* sequence is signal sequence, and following asterisks indicates probable plastid transit peptide. It is conceivable that these sequences compose apicoplast targeting signal. Targeting signals in the N-terminal were analyzed by SignalP [11] and PlasmoAP [12].

the manufacturer's recommendations. Pyruvate kinase isozyme purity was analyzed by SDS–PAGE on 8% polyacrylamide gel as described by Laemmli [5] (Data not shown). The recombinant protein concentration was determined by Bradford assay [6] using bovine serum albumin (BSA) as a standard.

Anti-recombinant *Pf*PyKII antibody was produced through a commercial company (Immuno-Biological Laboratories, Takasaki, Japan). Briefly, purified recombinant *Pf*PyKII from wheat germ extracts was used to immunize a BALB/c mouse. Following six injections of pyruvate kinase isozyme (5 µg each) at 1-week intervals, the whole IgG was isolated from peritoneal fluid with a HiTrap rProtein A FF column (GE Healthcare). The whole cell lysate of 1×10^8 erythrocytic stage *P. falciparum* parasites (FCR-3 strain) was separated on 8% acrylamide gel and blotted onto a nitrocellulose Hybond-C Extra membrane (GE Healthcare). The membrane was blocked for 20 min with 2% skimmed milk in Tris-buffered saline containing 0.2% Tween 20, incubated for 1 h with primary antibodies (1:3000), probed with alkaline phosphatase-conjugated goat anti-mouse IgG (Vector Laboratories, Burlingame, CA, USA) (1:5000), and detected with a BCIP-NBT system (Roche, Basel, Switzerland). Molecular sizes of the protein bands were determined with reference to pre-stained Rainbow molecular weight markers (GE Healthcare).

Cells were fixed and stained using the procedures described by Tonkin et al. [7]. Cells were briefly fixed with 4% EM grade paraformaldehyde (ProSciTech, Thuringowa, Queensland, Australia) and 0.0075% EM grade glutaraldehyde (ProSciTech) in phosphate-buffered saline (PBS) for 30 min. Fixed cells were washed once in PBS and permeated with 0.1% Triton X-100/PBS for 10 min. Cells were washed again and treated with 0.1 mg/ml of sodium borohydride ($NaBH_4$)/PBS for 10 min. Following another wash, cells were blocked in 3% BSA/PBS for 1 h. For staining anti-*Pf*PyKII antibody-binding structure and apicoplast, anti-*Pf*PyKII mouse antibody (diluted 1/1000) and anti-acyl carrier protein (ACP) rabbit antibody (diluted 1/500; gifted by Geoff McFadden, University of Melbourne, Australia) were added and allowed to bind for a minimum of 1 h in 3% BSA/PBS. AlexaFluor goat anti-mouse 594 (red) and anti-rabbit 488 (green) secondary antibodies (Invitrogen, Carlsbad, CA, USA) were added at 1:1000 dilution (in 3% BSA/PBS) and allowed to bind for 1 h, while cells settled onto a previously flamed cover slip coated with 1% polyethylenimine (PEI; Sigma, St Louis, MO, USA). For staining the anti-*Pf*PyKII antibody-binding structure and mitochondrion, citrate synthase-GFP construct (gifted by Geoff McFadden) transformed *P. falciparum* was used. Anti-*Pf*PyKII mouse antibody (diluted 1/1000) was added and allowed to bind for 1 h, followed by addition of AlexaFluor goat anti-mouse 488 (green) antibody and Cy5-conjugated anti-GFP rabbit (red) antibody (diluted 1/1000; Sigma) and allowed to bind for 1 h. Cells were mounted in 50% glycerol with 0.1 mg/ml of 1,4-diazabicyclo[2,2,2]octane (DABCO, Sigma). The microscopic system was a DeltaVision restoration system (Applied Precision, Washington, USA) on an Olympus IX70 inverted microscope equipped with a mercury vapor lamp (100 W) and appropriate barrier emission filters. Images were taken 0.2 µm apart and deconvolved using softWoRx Explorer Suite (Applied Precision).

The deduced amino acid sequence of *Pf*PyKII (NCBI Accession# NP_700836), exhibiting low overall identity (21%) to that of *Pf*PyKI (NCBI Accession# CAG25081), contained a pyruvate kinase signature (PROSITE; PS00110) as did other species and other consensus regions, such as multiple binding sites of ADP, PEP, and divalent cations (Fig. 1). Based on protein alignment, *Pf*PyKII was predicted to be a monovalent cation-independent enzyme. Most of the monovalent cation-binding sites were conserved; however, two binding sites, Thr^{113} and Glu^{117} (in *Felis catus* pyruvate kinase), were substituted by Ile and Lys, respectively. These substitutions are a common characteristic of monovalent cation-independent pyruvate kinases. We found three-specific long insertions in the middle of domain B, A2, and C of *Pf*PyKII, as in *Tg*PyKII. These insertions were different in length, but the insert positions were the same as in *Tg*PyKII.

Following six injections of pyruvate kinase isozyme at 1-week intervals, the whole IgG was isolated from mouse peritoneal fluid. Western blot analysis showed a single band (~80 kDa) in the *P. falciparum* lysate (Fig. 2), which was different from the mass in the type-I enzyme (55.6 kDa), indicating no cross-reaction with the type-I enzyme. Preimmune serum detected no bands in the 1×10^8 *P. falciparum* lysate (data not shown). The antibody was used in immunofluorescence microscopy.

The stained structure from the anti-*Pf*PyKII antibody in *P. falciparum* merged into the apicoplast stained pattern (Fig. 3A), suggesting that *Pf*PyKII localizes to the apicoplast. To determine if *Pf*PyKII localizes to the mitochondria, we analysed the immunolocalization of *Pf*PyKII in a *P. falciparum* cell line expressing the citrate synthase fused to GFP, which targets to the mitochondria [7] (Fig. 3B). The merged image showed that anti-*Pf*PyKII stain is adjacent to, but not associated with, the mitochondria. The two stains were distinguishable in all the stages (data not shown). Thus, we concluded that *Pf*PyKII localizes to the apicoplast, not to the mitochondrion. The data indicate a different localization of type-II pyruvate kinase in *P. falciparum* from that in *T. gondii*.

A recombinant protein of *P. falciparum* pyruvate kinase type-II isozyme (*Pf*PyKII) was created using a wheat germ cell-free system. All our previous attempts for production of this recombinant protein in *E. coli* systems have failed. Probably, it was due to its biased codon usage. The efficiency of production of the protein in our study was not high; nevertheless, the wheat germ cell-free system is useful for creation of the recombinant protein.

In addition, we showed localization of *Pf*PyKII in the apicoplast by immunofluorescent assay. Despite its proteobacterial origin, *Pf*PyKII was localized only to the apicoplast, not to the mitochondrion as in *Tg*PyKII, which is localized to both the mitochondrion and the apicoplast. The difference in metabolic pathways in the organelles between *T. gondii* and *P. falciparum* might reflect differences in their internal environment and in the metabolic relationships between those organelles in the two parasites. Further investigation to reveal these potential differences will contribute to understanding survival of *T. gondii* and *P. falciparum* in the host.

As suggested by Ralph et al. [8], pyruvate kinase in the apicoplast might dephosphorylate PEP imported into the apicoplast via PEP transporter on the apicoplast membrane and supply pyruvate for fatty acid synthesis and the non-mevalonate 1-deoxy-D-xylulose-5-phophate (DOXP) pathway in the organelle. Fleige et al. [9], reporting on carbohydrate metabolism in the *T. gondii* apicoplast, indicated that TgPykII was localized in the apicoplast. These findings suggest differences between *T. gondii* and *P. falciparum* in the mitochondrion and apicoplast metabolic pathways, even though *T. gondii*

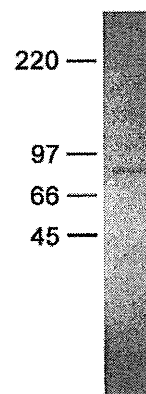

Fig. 2. Specificity of anti-*Pf*PyKII IgG shown by Western blot analysis. The purified recombinant *Pf*PyKII was detected by Western blot analysis with the antibody against the recombinant *Pf*PyKII. Rainbow molecular weight markers (kDa) are indicated on the left.

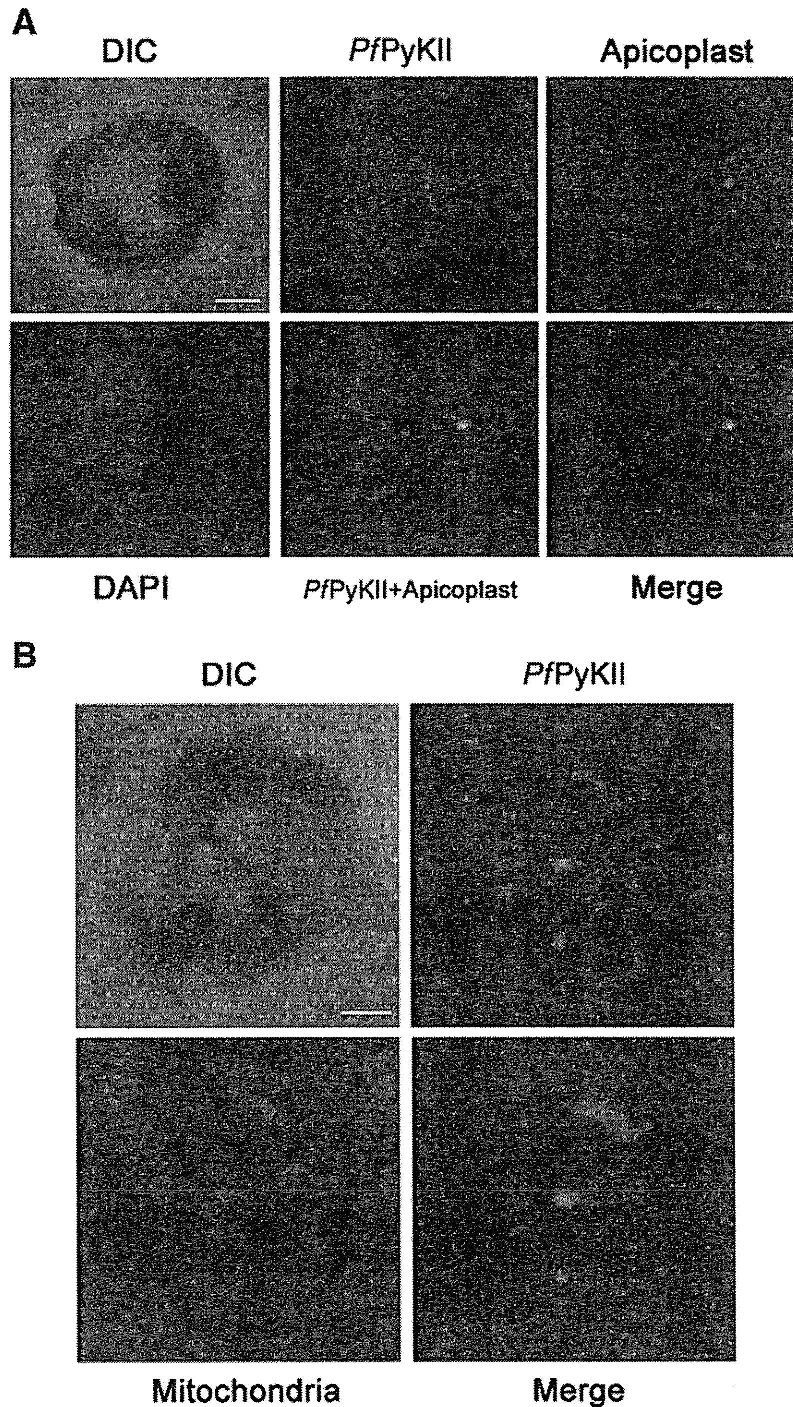

Fig. 3. Immunofluorescent microscopic analysis of co-localization of *Pf*PyKII with the apicoplast, but not with the mitochondrion in red blood cells infected with *P. falciparum*. A: Anti-*Pf*PyKII and anti-*P. falciparum* ACP antibodies detected by AlexaFlour goat anti-mouse 594 (red) and goat anti-rabbit 488 (green) secondary antibodies, respectively. Immunofluoresecnce of *P. falciparum* ACP antibody shows the apicoplast. Merged images indicate co-localization of *Pf*PyKII and *P. falciparum* ACP. Nucleus stained by DAPI (blue). B: Red blood cells infected with parasites expressing citrate synthase fused to GFP targeting the mitochondrion (Tonkin et al. 2004). GFP detected by Cy5-conjugated goat anti-GFP (red). Anti-*Pf*PyKII antibody detected by AlexaFluor goat anti-mouse 488 (green) IgG. Merged image shows that *Pf*PyKII does not co-locate with the mitochondrion. White scale bars are 2 μm.

and *P. falciparum* have comparable organelle components, and were thought to have similar enzyme components in both the apicoplast and the mitochondrion. The pathway differences might reflect differences in intracellular environments or different abilities to import metabolites into those organelles. We expected that the difference in enzymatic properties between *Tg*PyKII and *Pf*PyKII would help in understanding their roles in the two parasites, but several attempts to express the active recombinant enzyme have failed. As pyruvate kinase has been thought to play a role only in glycolysis in the cytosol, pyruvate kinases localized with cell organelles are unique. Non-glycolytic pyruvate kinases have been found only in the apicomplexan parasites, such as *Plasmodium* sp,

Theileria sp, and *T. gondii*. Characterization of non-glycolytic pyruvate kinases would increase the understanding of the unique metabolic pathways in protozoan parasites.

In addition to uncertainty about metabolic pathways, we are also uncertain about the origin of *Pf*PyKII. Although *Pf*PyKII exhibits a typical bipartite signal in the N-terminus, *Pf*PyKII has a proteobacterial origin, which is indicative of the apicoplast protein, and not a cyanobacterial or plastidic origin [2]. We suggest that *Pf*PyKII might have been obtained from endosymbiotic bacteria. Originally *Pf*PyKII may have localized in both the mitochondrion and the apicoplast, as in *T. gondii*; subsequently *P. falciparum* may have lost the mitochondrial location during evolutionary development.

Acknowledgements

We thank Dr. Shinichiro Kawazu (Obihiro University of Agriculture and Veterinary Medical) for providing genomic DNA of *P. falciparum*, and Dr. Geoffrey I. McFadde (University of Melbourne) for providing both anti-acyl carrier protein rabbit antibody and *P. falciparum* expressing citrate synthase fused to GFP. This work was supported in part by Keio Gijuku Academic Development Funds, Japan.

References

[1] Maeda T, Saito T, Oguchi Y, Nakazawa M, Takeuchi T, Asai T. Expression and characterization of recombinant pyruvate kinase from *Toxoplasma gondii* tachyzoites. Parasitol Res 2003;89:259–65.

[2] Saito T, Nishi M, Lim MI, Wu B, Maeda T, Hashimoto H, Takeuchi T, Roos DS, Asai T. A novel GDP-dependent pyruvate kinase isozyme from *Toxoplasma gondii* localizes to both the apicoplast and the mitochondrion. J Biol Chem 2008;283:14041–52.

[3] Chan M, Sim TS. Functional analysis, overexpression, and kinetic characterization of pyruvate kinase from *Plasmodium falciparum*. Biochem Biophys Res Commun 2004;326:188–96.

[4] Sawasaki T, Gouda MD, Kawasaki T, Tsuboi T, Tozawa Y, Takai K, Endo Y. The wheat germ cell-free expression system: methods for high-throughput materialization of genetic information. Methods Mol Biol 2005;310:131–44.

[5] Laemmli UK. Cleavage of structural proteins during the assembly of the head of bacteriophage T4. Nature 1970;227:680–5.

[6] Bradford MM. A rapid and sensitive method for the quantitation of microgram quantities of protein utilizing the principle of protein–dye binding. Anal Biochem 1979;72:248–54.

[7] Tonkin CJ, van Dooren GG, Spurck TP, Struck NS, Good RT, Handman E, Cowman AF, McFadden GI. Localization of organellar proteins in *Plasmodium falciparum* using a novel set of transfection vectors and a new immunofluorescence fixation method. Mol Biochem Parasitol 2004;137:13–21.

[8] Ralph SA, van Dooren GG, Waller RF, Crawford MJ, Fraunholz MJ, Foth BJ, Tonkin CJ, Roos DS, McFadden GI. Tropical infectious diseases: metabolic maps and functions of the *Plasmodium falciparum* apicoplast. Nat Rev Microbiol 2004;2:203–16.

[9] Fleige T, Fischer K, Ferguson DJP, Gross U, Bohne W. Carbohydrate metabolism in the *Toxoplasma gondii* apicoplast: localization of three glycolytic isoenzymes, the single pyruvate dehydrogenase complex, and a plastid phosphate translocator. Eukaryot Cell 2007;6:984–96.

[10] Rigden DJ, Phillips SE, Michels PA, Fothergill-Gilmore LA. The structure of pyruvate kinase form *Leishmania mexicana* reveals details of the allosteric transition and unusual effector specificity. J Mol Biol 1999;291:615–35.

[11] Bendtsen JD, Nielsen H, von Heijne G, Brunak S. Improved prediction of signal peptides: SignalP 3.0. J Mol Biol 2004;340:783–95.

[12] Foth BJ, Ralph SA, Tonkin CJ, Struck NS, Fraunholz M, Roos DS, Cowman AF, McFadden GI. Dissecting apicoplast targeting in the malaria parasite *Plasmodium falciparum*. Science 2003;299(5607):705–8.

Parasitology International 58 (2009) 196–199

Contents lists available at ScienceDirect

Parasitology International

journal homepage: www.elsevier.com/locate/parint

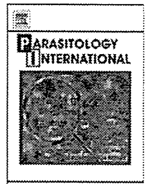

Short communication

A small-scale systematic analysis of alternative splicing in *Plasmodium falciparum*

Hideyuki Iriko [a,b,c], Ling Jin [a,b], Osamu Kaneko [d,e], Satoru Takeo [b], Eun-Taek Han [b,f], Mayumi Tachibana [d], Hitoshi Otsuki [d], Motomi Torii [d], Takafumi Tsuboi [a,b,*]

[a] *Venture Business Laboratory, Ehime University, Matsuyama, Ehime 790-8577, Japan*
[b] *Cell-Free Science and Technology Research Center, Ehime University, Matsuyama, Ehime 790-8577, Japan*
[c] *Department of Microbiology and Pathology, Faculty of Medicine, Tottori University, Yonago, Tottori 683-8503, Japan*
[d] *Department of Molecular Parasitology, Ehime University Graduate School of Medicine, Toon, Ehime 791-0295, Japan*
[e] *Department of Protozoology, Institute of Tropical Medicine (NEKKEN), Nagasaki University, Sakamoto, Nagasaki 852-8523, Japan*
[f] *Department of Parasitology, Kangwon National University College of Medicine, Chunchon 200-701, Republic of Korea*

ARTICLE INFO

Article history:
Received 6 November 2008
Received in revised form 30 January 2009
Accepted 15 February 2009
Available online 5 March 2009

Keywords:
Alternative splicing
Exon definition
Gametocyte
Malaria
Plasmodium falciparum

ABSTRACT

During the last decade transcriptome analyses demonstrated that alternative splicing plays an important role to generate a large number of mRNA and protein isoforms from a limited number of genes. However, the frequency of the alternative splicing dramatically varies among living organisms. For example, 35–65% of human genes are involved in alternative splicing, whereas only a few are reported for unicellular organism yeast. Alternative splicing has been observed for several genes in the deadliest malaria parasite *Plasmodium falciparum*, but the frequency and the type were not systematically analyzed so far. In this study, we determined partial cDNA sequences for 88 open reading frames surrounding 246 introns in *P. falciparum* which were transcribed at schizont and gametocyte stages, and observed 15 instances of alternative splicing within a total of 14 gene transcripts, 16% of the analyzed genes. Among 5 basic splicing patterns, alternative 5′ and 3′ splicing, and intron retention were detected. Alternative splicing in 7 open reading frames had effects on the domain architectures of the gene products, which might result in modifying the cellular localization and function of these products.

© 2009 Elsevier Ireland Ltd. All rights reserved.

Malaria is a significant human disease of global concern that causes several million deaths annually, as well as hundreds of millions of episodes of clinical illness. The intricate life cycle of the pathogenic protozoan agent of malaria, *Plasmodium*, belays an extraordinary biological complexity that underlies its development in both a warm-blooded host and mosquito vector. The parasite has the capacity to recognize and infect multiple cell types, such as salivary glands, hepatocytes, and erythrocytes; and has three distinct motile or invasive stages that traverse different tissues before infecting a new host cell [1]. In comparison to the simple unicellular yeasts, which are predicted to have ~5000 genes [2], the estimated size of the *Plasmodium* genome appears to inadequately reflect the remarkable biological complexity of its life cycle. The *Plasmodium falciparum* genome is estimated to have ~6000 genes, and the complexity of unique genes is considerably less due to the amplification of numerous multi-gene families, such as *var*, *rif*, and *stevor* [3], that occupy a significant part of the *Plasmodium* genome.

During the last decade transcriptome analyses demonstrated that alternative splicing plays an important role to generate a large number of mRNA and protein isoforms from a limited number of genes [4,5]. However, the frequency of the alternative splicing dramatically varies among living organisms. For example, 35–65% of human genes are involved in alternative splicing, whereas only a few are reported for yeast [4], despite the observation of 4730 predicted introns that are encoded within *Schizosaccharomyces pombe* genes [2]. In *P. falciparum*, 7406 introns were predicted in the genome, whereas alternative splicing has been observed only for a few genes that might affect protein function. For example, adenylyl cyclase variant isoforms may have functional differences [6]; and MAEBL variant isoforms are suggested to change the type I membrane product to a soluble isoform [7]. Another example is the stromal-processing peptidase and delta-aminolevulinic acid dehydratase, which share a common apicoplast-targeting leader sequence via the skipping of 4 intervening exons [8]. Alternative splicing was also reported for the blood stage antigen 41-3 precursor [9]; CDK-related protein kinase 6 [10]; and an aspartyl protease [11]. Thus, alternative splicing does occur in *Plasmodium*; however, the information is largely anecdotal and the prevalence of this mechanism remains unclear. Since alternative splicing can profoundly affect estimations of the breadth and complexity of the proteome (mRNA sequences) from the genome nucleotide sequence information, algorithms predictive of alternative splicing are increasingly needed. Indeed, we have observed in *P. falciparum* that alternatively spliced transcripts are not as rare as the anecdotal evidence would suggest, in the course of our experiences performing high-throughput cloning of protein expression constructs using cDNA templates [12]. In this report, we summarize our data and

Abbreviations: ORF, open reading frame.

* Corresponding author. Venture Business Laboratory, Ehime University, Matsuyama, Ehime 790-8577, Japan. Tel.: +81 89 927 8277; fax: +81 89 927 9941.
E-mail address: tsuboi@ccr.ehime-u.ac.jp (T. Tsuboi).

1383-5769/$ – see front matter © 2009 Elsevier Ireland Ltd. All rights reserved.
doi:10.1016/j.parint.2009.02.002

assess the frequency and the type of alternative splicing in *P. falciparum*; and predict the effect of altered transcripts on the localization and function of the produced proteins. Moreover, we provide evidence that the protozoan *P. falciparum* possesses both exon- and intron-recognition systems that initiate intron splicing.

The *P. falciparum* NF54 line was maintained in culture as described [13]. Asynchronous parasites were collected, and the erythrocytes were removed by saponin-mediated lysis. Parasite pellets were washed with phosphate buffered saline, and stored at −80 °C until use. Gametocyte stages were induced by maintaining parasite cultures at 37 °C using a gas mixture (90% N_2, 5% O_2, and 5% CO_2) for an extended period of time without the addition of fresh erythrocytes, and fully matured gametocytes were collected, washed in phosphate buffered saline, and stored at −80 °C until use. Sixty-nine % of the parasites were fully matured stage V gametocytes. Total RNA was extracted from parasite pellets using the RNeasy mini kit (Qiagen, Valencia, CA), and RNA preparations were extensively treated with DNase I to remove contaminating DNA. cDNA was prepared using Superscript III reverse-transcriptase (RT; Invitrogen, Carlsbad, CA). Open reading frames (ORFs) transcribed at schizont and gametocyte stages were selected for the analysis based on the transcriptome analysis [14]. Oligonucleotide primers were designed based upon annotated sequences in PlasmoDB [15], in order to PCR amplify predicted full-length ORFs. Eighty-eight ORFs were amplified by RT-PCR and cloned into the pCR2.1-TOPO TA plasmid (Invitrogen). Nucleotide sequence of the inserts were determined for 2 to 8 clones for each ORF using an ABI PRISM® 310 and 3100 Genetic Analyzers (Applied Biosystems, Foster City, CA) with M13(-20) and M13 reverse primers.

In this manner we randomly determined partial cDNA sequences for 88 ORFs surrounding 246 introns. The distribution of the ORFs arranged according to stage-specificity of the transcriptional cluster [14] and the number of the constituent introns are described in greater detail in Table 1. Similar to most other eukaryotes, exon boundaries of *Plasmodium* are demarcated by consensus donor and acceptor splicing junctions, GU and AG, respectively [16]. We observed 15 instances of alternative splicing within a total of 14 gene transcripts, 16% of the analyzed 88 genes (Table 1 and Supplementary Table 1). Because we only sequenced 2 to 8 clones for each intron, this value should be taken as a minimal estimation, and the true frequency of the alternative splicing is expected to be higher. To evaluate the alternative splicing in other strain, we performed RT-PCR analysis using gametocyte pellet purified from a malaria patient blood obtained from malaria endemic area in Mae Sot, Thailand. We checked 7 genes specifically expressed at gametocyte stage (PFE0220w, MAL8P1.149, MAL13P1.85, MAL13P1.211, PFD0700c, PF13_0220, and PFE0680w). As a result, five genes (PFE0220w, MAL8P1.149, MAL13P1.85, PFD0700c, and PF13_0220) also showed alternatively spliced variants together with the predicted parent transcripts as NF54 (data not shown). These results suggest that alternative splicing also occur in naturally isolated *P. falciparum* parasites. It was shown that alternative splicing in *P. falciparum* is a higher level than expected, based on the rarity of alternative splicing events in *S. pombe* [4].

The observed alternative splicing events were classified into 3 types: alternative 5′ splicing (46.7% of cases); alternative 3′ splicing (26.7% of cases); and intron retention/creation (26.7% of cases) (Fig. 1A). Notably, this is the first evidence of alternative 5′ splicing in *P. falciparum*. Another type of alternative splicing is exon skipping, which is the most prominent splicing pattern in metazoans; for example, 38% of events in humans are due to exon skipping [4,5]. Although 3 cases of exon skipping have been reported in *P. falciparum* [6,8,9], we did not observe this type occurring in this study.

Table 1
Analyzed *Plasmodium falciparum* introns in this study.

Cluster[a]	Stage[b]	Total		Alternative splicing	
		ORFs	Introns	ORFs (%)	Introns (%)
3	Gm	42	160	8 (19.0%)	9 (6.0%)
4	R/Sch/Mz	16	18	2 (12.5%)	2 (11.8%)
13	Sch/Gm	2	2	0 (0.0%)	0 (0.0%)
14	Spz/Sch/Gm	6	13	2 (33.3%)	2 (15.4%)
15	Sch	22	53	2 (9.1%)	2 (3.8%)
Total		88	246	14 (16.0%)	15 (6.4%)

[a] Open reading frames (ORF) were clustered based on the transcription pattern [14].
[b] Gm, gametocyte; R, ring; Sch, schizont; Mz, merozoite; Spz, sporozoite.

To assess the effect of the predicted alternative protein products, we analyzed the domain architectures of the splicing variants. Alternative splicing in 7 ORFs (MAL13P1.211, PFE0220w, PF13_0220, PF10_0021, PFD0700c, PF14_0694, and PFI0110c) had effects on the domain architectures of the gene products (Fig. 1B). The predicted parent transcripts (type 1) of MAL13P1.211 and PFE0220w encode proteins which possess a single transmembrane domain at their C-termini; whereas the alternatively spliced products harbored a frameshift and an early stop codon that resulted in truncated proteins lacking transmembrane domains. The cellular localization is therefore likely to depend on the splicing status, and the presence or absence of a transmembrane domain. Other transcripts (type 1) corresponding to PFD0700c, PF14_0694, and PFI0110c possessed at their C-termini an RNA recognition motif, thioredoxin motif, and protein kinase domain, respectively; whereas alternatively spliced variants (type 2) lacked these domains either partially or completely, suggesting that the protein functions would be abolished or suppressed. Although no known functional domains were detected for PF13_0220 or PF10_0021, the type 2 transcripts encode stop codons approximately 20 to 30 amino acids from the start codon, indicating that their expression as mature forms would be abolished.

Interestingly, among the two types of transcripts showing 5′ alternative splicing in *P. falciparum* the transcripts that encoded truncated product (type 2) almost always possessed a splicing site at the 5′ side compared to the predicted parent transcripts (type 1). This suggests that splicing site at 3′ side is original and that a cryptic splice site was activated in the preceding exon, likely weak splicing signal of the original site. In unicellular eukaryote yeast, mutations in splice sites lead to the activation of cryptic splice sites located downstream of the mutated site, suggesting that splicing machineries initially recognize intron (intron definition) [17]. However, in the metazoans, mutations in splice sites typically lead to the activation of cryptic splice sites located in the preceding exon or exon skipping [18], suggesting that the exon is primarily recognized (exon definition). Thus the pattern observed for *P. falciparum* fits to the "exon definition". Furthermore, 3 cases of exon skipping reported in *P. falciparum* support the presence of the "exon definition" system in this protist [6,8,9]. Because the observed intron retentions suggest the presence of "intron definition" system, *P. falciparum* appears to initiate splicing via both "exon definition" and "intron definition" systems. This is similar to the metazoan, *Drosophila melanogaster*, for which both intron retention and exon skipping have been observed [19,20].

In this study, we found frequent 5′ alternative splicing, however this type has never been reported in *P. falciparum* despite well over a decade of molecular cloning history of numerous *P. falciparum* genes. This might be explained by our cloning strategy to target gametocyte transcripts rather than asexual stage transcripts (Fig. 1). Because the *Plasmodium* female gametocyte was shown to translationally repress specific mRNA species by forming a complex in the cytoplasm to store mRNA for translation after fertilization [21], there might be a relation between these two observations via mRNA binding proteins. In all eukaryotes, splicing is mediated by a macromolecular spliceosome machinery that consists of small nuclear ribonucleoproteins (snRNPs) and non-snRNP splicing factors with RNA binding motif, including serine–arginine-rich (SR) proteins. Among SR proteins, SF2/ASF shows multiple functions, one of which is to affect alternative splice site selection by antagonizing other SR proteins, such as SC35 and SRp20 [22,23]. SF2/ASF is also reported to associate with ribosomes to stimulate translation [24]. Such concerted regulation of nuclear and

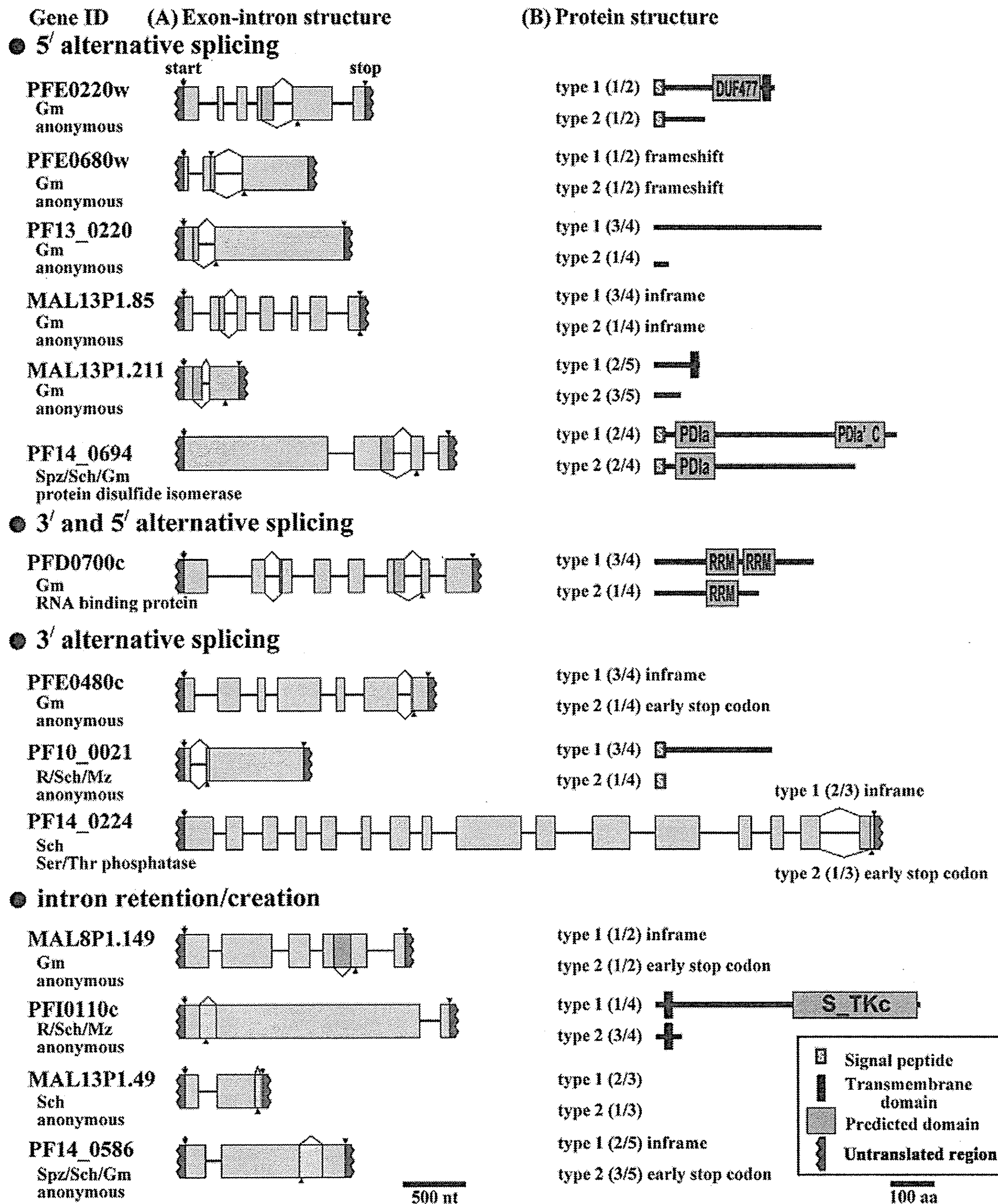

Fig. 1. Alternative splicing events that were detected in this study for *Plasmodium falciparum*. (A) Exon–intron boundaries for 2 types of transcripts are shown. Arrows indicate probable start codons. Arrowheads at the top or the bottom of each schematic indicate probable stop codons according to the exon–intron boundaries. Stage that transcribes each gene is shown under the Gene ID according to the transcriptome analysis [14]; Gm, gametocyte; Sch, schizont; R, ring; Mz, merozoite; Spz, sporozoite. Protein annotations refer to PlasmoDB [15]. (B) Predicted domain architectures of the proteins encoded by two variant transcripts. Type 1 is the presumed original transcript that encodes a longer open reading frame, whereas type 2 encodes a truncated product. The number of the clones for each type, per total clones, is shown in parentheses. Signal peptides and transmembrane domains were predicted by the SignalP and TMHMM2 programs, respectively. Domains were predicted by the SMART program (http://smart.embl-heidelberg.de/) or by searching the Conserved Domain Database (CDD) with Reverse Position Specific BLAST. Domains include: unknown function 477 (DUF477); thioredoxin domain of protein disulfide isomerase family (PDIa); C-terminal thioredoxin domain PDIa' subfamily (PDIa'_C); Ser/Thr protein kinase motif (S_TKc); and the RNA recognition motif (RRM). The type of alternative splicing for the MAL8P1.149 is likely intron creation rather than intron retention, because type 1 possesses another intron and encoding longer open reading frame.

cytoplasmic activities of SR proteins was shown in mammalian cells [25]. A putative *P. falciparum* ortholog of SF2/ASF (PFE0865c and PF11_0205) might affect alternative splicing in *Plasmodium*. Interestingly, most of the *P. falciparum* genes reported to show alternative splicing are transcribed at the gametocyte and/or sporozoite stages [16], and this observation does not contradict our proposal.

In summary, among 88 isolated genes we found 14 genes that showed alternative splicing patterns, and half of these resulted in an alteration of the protein domain architecture. Splicing machinery initially recognized introns in *P. falciparum*, as suggested by the presence of intron retention, similar to the other unicellular eukaryote yeast. In addition, the pattern of alternative 5′ splicing, in combination with previous reports of the exon skipping, suggests that the exon is also recognized to initiate splicing in *P. falciparum*. This is an important observation, because unicellular eukaryotes are proposed to possess only an "intron definition" system, based on the data from yeast.

Acknowledgements

We thank T. Templeton for critical reading of the manuscript. Gametocyte rich cultures of *Plasmodium falciparum* were a kind gift from C. Long. This work was supported in part by Grants-in-Aid for Scientific Research 18390129 and 19406009 (to T. T.); Scientific Research on Priority Areas 19041053 (to T. T.) from the Ministry of Education, Culture, Sports, Science, and Technology, Japan; and, in part, by a Grant-in-Aid of the Ministry of Health, Labour, and Welfare (H20-Sinkou-ippan-013), Japan (to T. T.).

Appendix A. Supplementary data

Supplementary data associated with this article can be found, in the online version, at doi:10.1016/j.parint.2009.02.002.

References

[1] Markell EK, John DT, Krotoski WA. Medical parasitology. 8th ed. Philadelphia: WB Saunders; 1998.
[2] Wood V, Gwilliam R, Rajandream MA, Lyne M, Lyne R, Stewart A, et al. The genome sequence of *Schizosaccharomyces pombe*. Nature 2002;415:871–80.
[3] Gardner MJ, Hall N, Fung E, White O, Berriman M, Hyman RW, et al. Genome sequence of the human malaria parasite *Plasmodium falciparum*. Nature 2002;419:498–511.
[4] Ast G. How did alternative splicing evolve? Nat Rev Genet 2004;5:773–82.
[5] Stamm S, Ben-Ari S, Rafalska I, Tang Y, Zhang Z, Toiber D, et al. Function of alternative splicing. Gene 2005;344:1–20.
[6] Muhia DK, Swales CA, Eckstein-Ludwig U, Saran S, Polley SD, Kelly JM, et al. Multiple splice variants encode a novel adenylyl cyclase of possible plastid origin expressed in the sexual stage of the malaria parasite *Plasmodium falciparum*. J Biol Chem 2003;278:22014–22.
[7] Singh N, Preiser P, Rénia L, Balu B, Barnwell J, Blair P, et al. Conservation and developmental control of alternative splicing in *maebl* among malaria parasites. J Mol Biol 2004;343:589–99.
[8] van Dooren GG, Su V, D MC, Ombrain, McFadden GI. Processing of an apicoplast leader sequence in *Plasmodium falciparum* and the identification of a putative leader cleavage enzyme. J Biol Chem 2002;277:23612–9.
[9] Knapp B, Nau U, Hundt E, Kupper HA. Demonstration of alternative splicing of a pre-mRNA expressed in the blood stage form of *Plasmodium falciparum*. J Biol Chem 1991;266:7148–54.
[10] Bracchi-Ricard V, Barik S, Delvecchio C, Doerig C, Chakrabarti R, Chakrabarti D. PfPK6, a novel cyclin-dependent kinase/mitogen-activated protein kinase-related protein kinase from *Plasmodium falciparum*. Biochem J 2000;347:255–63.
[11] Volkman SK, Barry AE, Lyons EJ, Nielsen KM, Thomas SM, Choi M, et al. Recent origin of *Plasmodium falciparum* from a single progenitor. Science 2001;293:482–4.
[12] Tsuboi T, Takeo S, Iriko H, Jin L, Tsuchimochi M, Matsuda S, et al. Wheat germ cell-free system-based production of malaria proteins for discovery of novel vaccine candidates. Infect Immun 2008;76:1702–8.
[13] Trager W, Jensen JB. Human malaria parasites in continuous culture. Science 1976;193:673–5.
[14] Le Roch KG, Zhou Y, Blair PL, Grainger M, Moch JK, Haynes JD, et al. Discovery of gene function by expression profiling of the malaria parasite life cycle. Science 2003;301:1503–8.
[15] Bahl A, Brunk B, Crabtree J, Fraunholz MJ, Gajria B, Grant GR, et al. PlasmoDB: the *Plasmodium* genome resource. A database integrating experimental and computational data. Nucleic Acids Res 2003;31:212–5.
[16] Vinkenoog R, Veldhuisen B, Speranҫa MA, del Portillo HA, Janse C, Waters AP. Comparison of introns in a cdc2-homologous gene within a number of *Plasmodium* species. Mol Biochem Parasitol 1995;71:233–41.
[17] Romfo CM, Alvarez CJ, van Heeckeren WJ, Webb CJ, Wise JA. Evidence for splice site pairing via intron definition in *Schizosaccharomyces pombe*. Mol Cell Biol 2000;20:7955–70.
[18] Berget SM. Exon recognition in vertebrate splicing. J Biol Chem 1995;270:2411–4.
[19] Talerico M, Berget SM. Intron definition in splicing of small *Drosophila* introns. Mol Cell Biol 1994;14:3434–45.
[20] Shen J, Zu K, Cass CL, Beyer AL, Hirsh J. Exon skipping by overexpression of a *Drosophila* heterogeneous nuclear ribonucleoprotein in vivo. Proc Natl Acad Sci USA 1995;92: 1822–5.
[21] Mair GR, Braks JA, Garver LS, Wiegant JC, Hall N, Dirks RW, et al. Regulation of sexual development of *Plasmodium* by translational repression. Science 2006;313:667–9.
[22] Jumaa H, Nielsen PJ. The splicing factor SRp20 modifies splicing of its own mRNA and ASF/SF2 antagonizes this regulation. EMBO J 1997;16:5077–85.
[23] Gallego ME, Gattoni R, Stevenin J, Marie J, Expert-Bezancon A. The SR splicing factors ASF/SF2 and SC35 have antagonistic effects on intronic enhancer-dependent splicing of the beta-tropomyosin alternative exon 6A. EMBO J 1997;16:1772–84.
[24] Sanford JR, Gray NK, Beckmann K, Caceres JF. A novel role for shuttling SR proteins in mRNA translation. Genes Dev 2004;18:755–68.
[25] Blaustein M, Pelisch F, Tanos T, Muñoz MJ, Wengier D, Quadrana L, et al. Concerted regulation of nuclear and cytoplasmic activities of SR proteins by AKT. Nat Struct Mol Biol 2005;12:1037–44.

Single amino acid substitution in *Plasmodium yoelii* erythrocyte ligand determines its localization and controls parasite virulence

Hitoshi Otsuki[a], Osamu Kaneko[a,b,1], Amporn Thongkukiatkul[a,c], Mayumi Tachibana[a], Hideyuki Iriko[a,d], Satoru Takeo[e], Takafumi Tsuboi[e], and Motomi Torii[a]

[a]Department of Molecular Parasitology, Ehime University Graduate School of Medicine, Toon, Ehime 791-0295, Japan; [b]Department of Protozoology, Institute of Tropical Medicine (NEKKEN) and the Global Center of Excellence Program, Nagasaki University, Nagasaki, Nagasaki 852-8523, Japan; [c]Department of Biology, Burapha University, Amphur Muang, Chonburi 20131, Thailand; [d]Department of Microbiology and Pathology, Faculty of Medicine, Tottori University, Yonago, Tottori 683-8503, Japan; and [e]Cell-Free Science and Technology Research Center, Ehime University, Matsuyama, Ehime 790-8577, Japan

Edited by Thomas E. Wellems, National Institutes of Health, Bethesda, MD, and approved February 23, 2009 (received for review November 10, 2008)

The major virulence determinant of the rodent malaria parasite, *Plasmodium yoelii*, has remained unresolved since the discovery of the lethal line in the 1970s. Because virulence in this parasite correlates with the ability to invade different types of erythrocytes, we evaluated the potential role of the parasite erythrocyte binding ligand, *Py*EBL. We found 1 amino acid substitution in a domain responsible for intracellular trafficking between the lethal and nonlethal parasite lines and, furthermore, that the intracellular localization of *Py*EBL was distinct between these lines. Genetic modification showed that this substitution was responsible not only for *Py*EBL localization but also the erythrocyte-type invasion preference of the parasite and subsequently its virulence in mice. This previously unrecognized mechanism for altering an invasion phenotype indicates that subtle alterations of a malaria parasite ligand can dramatically affect host–pathogen interactions and malaria virulence.

dense granule | invasion | malaria | microneme | transfection

The rodent malaria parasite *Plasmodium yoelii yoelii* has been widely studied to understand the interactions between the malaria parasite and the host cell (1). The nonlethal 17X line mainly infects young erythrocytes (reticulocytes), whereas the lethal 17XL and YM lines infect a wide range of erythrocytes. These lines have previously been studied to identify the genetic determinants of virulence (2, 3). These differences in erythrocyte invasion preference suggest the possible involvement of a parasite ligand that recognizes erythrocyte surface receptors; however, the actual molecular basis of the observed invasion preference differences remains unclear.

Erythrocyte invasion by the malaria merozoite is a multistep process, initiated by reversible binding to the erythrocyte surface, followed by the establishment of a tight junction between the apical end of the merozoite and erythrocyte surface and the subsequent movement of the merozoite into the nascent parasitophorous vacuole. Each step involves specific interactions between parasite ligands and erythrocyte receptors. Among the ligands of malaria parasites, the best characterized is a type I integral transmembrane protein encoded by the *ebl* (*erythrocyte-binding-like*) gene family. Upon release from the micronemes, EBL proteins recognize erythrocyte receptors and initiate the formation of the tight junction. The importance of EBL in malaria virulence is exemplified in the human malaria parasite *Plasmodium vivax*, which uses an EBL orthologue, *Pv*DBP, to recognize the Duffy antigen on the erythrocyte surface. Because the parasite is apparently unable to use an alternative invasion pathway, individuals in whom the Duffy antigen is not expressed on the erythrocyte surface are completely resistant to *P. vivax* (4, 5). Because of this dramatic association between the disruption of a host–pathogen interaction and protection against a malaria parasite, *Pv*DBP and the *Plasmodium falciparum* EBL orthologue, EBA-175, have been targeted for vaccine development (6).

EBL proteins possess 2 Cys-rich regions conserved among EBL orthologues. The N-terminal Cys-rich region named the DBL (Duffy-binding-like) domain or region 2 (7) recognizes a specific erythrocyte surface receptor. The C-terminal Cys-rich region named the C-cys domain or region 6 is located adjacent to the transmembrane domain, and the number and location of Cys residues are well conserved among known *Plasmodium* species. Region 6 exhibits structural similarity to the KIX-binding domain of the coactivator CREB-binding protein (8) and has been proposed to be a protein trafficking signal for transportation to the micronemes (9). Here we report a single nonsynonymous nucleotide substitution in the *pyebl* gene between lethal and nonlethal lines of *P. yoelii* and show the effect of this substitution on the intracellular localization of EBL, erythrocyte-type preference, and consequently virulence of *P. yoelii*.

Results

To investigate differences in EBL between lethal and nonlethal *P. yoelii* lines, we compared sequences from a variety of malaria parasite species and *P. yoelii* lines 17X, 17XL, and YM. We found 1 nonsynonymous nucleotide substitution in region 6 between the nonlethal 17X and lethal 17XL lines in the entire ORF (Fig. 1). The nonlethal 17X line possesses 8 conserved Cys residues that form 4 disulfide bridges (8), whereas the lethal 17XL line possesses an Arg instead of Cys at the second Cys position. This substitution was also found in another lethal line, "YM" (2), which originated independently from the 17X line during serial passage (3). All *Plasmodium* EBL orthologues for which protein expression was validated possess 8 conserved Cys residues in this region, further indicating that these Cys residues play an important role (supporting information Fig. S1). Thus the observed substitution from Cys to Arg is likely to abolish the native conformation of region 6.

EBL Localizes in the Dense Granules in *P. yoelii* Line 17XL. We raised specific polyclonal and monoclonal antibodies against *Py*EBL

Author contributions: H.O., O.K., and M. Torii designed research; H.O., A.T., M. Tachibana, H.I., and S.T. performed research; T.T. contributed new reagents/analytic tools; H.O., O.K., and M. Torii analyzed data; and H.O. and O.K. wrote the paper.

The authors declare no conflict of interest.

This article is a PNAS Direct Submission.

Data deposition: The data reported in this article have been deposited in the GenBank/European Molecular Biology Laboratory/DNA Data Base in Japan databases (accession nos. AB430781–AB430789).

[1]To whom correspondence should be addressed. E-mail: okaneko@nagasaki-u.ac.jp.

This article contains supporting information online at www.pnas.org/cgi/content/full/0811313106/DCSupplemental.

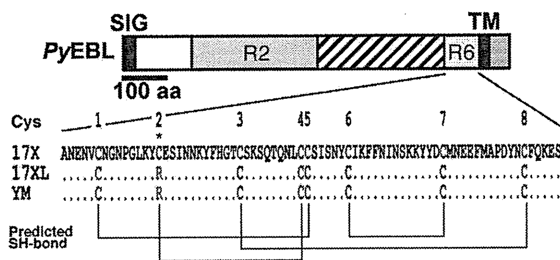

Fig. 1. Schematic structure of *P. yoelii* EBL (*Py*EBL). SIG, TM, R2, and R6 indicate the putative endoplasmic reticulum transporting signal, the transmembrane region, region 2, and region 6, respectively. Amino acid alignment of *Py*EBL from 17X, 17XL, and YM lines are shown below. Eight conserved Cys residues that form disulfide bridges (Predicted SH-bond) and the substitution from Cys to Arg (*) are indicated.

and performed Western blot analysis. The *Py*EBL protein was detected as a 110-kDa band in both the 17X and 17XL lines (Fig. 2*A*). The intracellular localization of *Py*EBL in both the 17X and 17XL lines was compared by indirect immunofluorescent assay

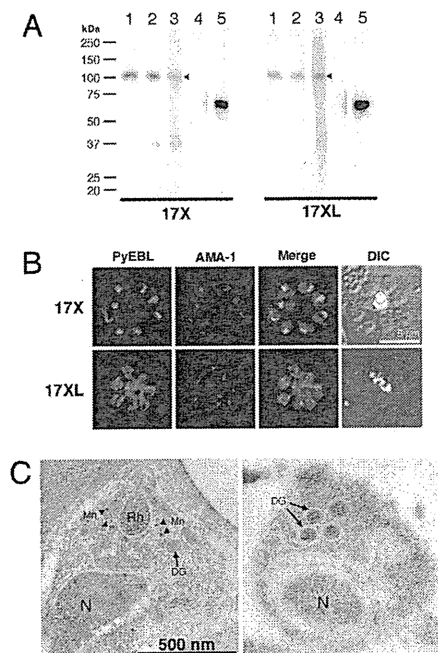

Fig. 2. Western blot analysis and *Py*EBL localization in *P. yoelii* schizont by immunostaining. (*A*) Western blot analysis with mAb 5B10 (lane 1), mAb 1G10 (lanes 2), and mouse serum (lane 3) specific for *Py*EBL against purified *P. yoelii* schizont extracts. A 110-kDa band was detected in both 17X and 17XL lines, with no significant difference in the protein expression level (arrowheads). This band was not detected by normal mouse serum (lane 4). Anti-AMA1 serum detected a 66-kDa band at similar levels (lane 5). (*B*) *P. yoelii* schizonts were incubated with mAb 5B10 (PyEBL), rabbit anti-AMA1 serum (AMA1), and DAPI (blue) for nuclear staining. Schizonts labeled with anti-*Py*EBL (5B10) were stained with FITC secondary antibody (green). Anti-AMA1 were stained with Alexa-546 secondary antibody (red). DIC images are shown in the right-hand column. The 17X line shows apical *Py*EBL signal colocalized with AMA1, but the region 6–substituted 17XL line shows diffused staining that does not colocalize with AMA1. (*C*) Immunoelectron microcopy was carried out for resin-embedded *P. yoelii* 17X and 17XL lines with anti-*Py*EBL mouse serum and secondary antibody conjugated with gold particles. *Py*EBL was detected in the micronemes (arrowheads) of the 17X line, but in the 17XL line it was located in the dense granules (arrows). N, nucleus; Mn, microneme; DG, dense granule; Rh, rhoptry.

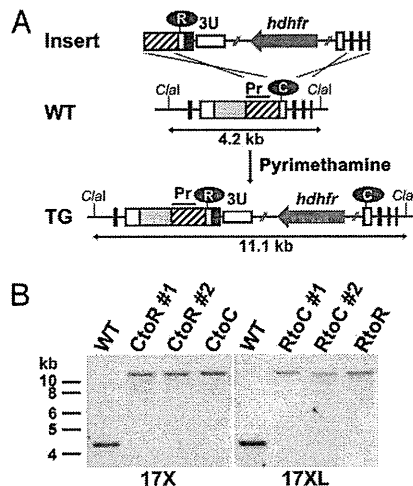

Fig. 3. Amino acid replacement of *Py*EBL region 6 second cysteine location by targeted recombination. (*A*) Schematic representation of the WT and modified (TG) *pyebl* gene loci. The replacement cassette (Insert) was inserted into the *pyebl* gene locus by double-crossover recombination. In this schematic, the second Cys in region 6 was replaced with Arg in the 17X line to generate 17X-CtoR. Other transgenic lines were generated in a similar fashion. ClaI restriction sites and the expected size of the DNA fragment after ClaI digestion are shown. Pr, probe region used in Southern blot analysis. (*B*) Southern blot analysis of the *pyebl* gene locus in WT and transgenic parasite lines derived from *P. yoelii* 17X and 17XL. The absence of the 4.2-kb WT band and the presence of an 11.1-kb band indicate that the *Py*EBL locus was modified in all transgenic clones.

(IFA) using specific antibodies against *Py*EBL (Fig. S2). In the 17X line, *Py*EBL localized to the apical end of each merozoite in both the segmented schizont-stage parasite and individual merozoites, where it colocalized with AMA1, a known microneme protein, under immunofluorescent microscopy (Fig. 2*B*). However, in the 17XL line *Py*EBL did not colocalize with AMA1 at the apical end of merozoites and showed a more diffused but granular distribution in comparison with parasites of the 17X line (Fig. 2*B*). Diffused localization of *Py*EBL was also observed in parasites of the YM line (Fig. S3). Immunoelectron microscopy revealed that *Py*EBL localized in micronemes in the 17X line as reported for *P. falciparum* and *Plasmodium knowlesi* (10, 11). In the 17XL line, however, *Py*EBL localized not in the microneme but in another microorganelle—the dense granules (12) (Fig. 2*C* and Fig. S4).

Because there seems to be only 1 copy of *Py*EBL in the genomes of both lines (Fig. S5), and significant differences were not observed in the level of transcription and protein expression between the 17X and 17XL lines (Fig. 2*A* and Fig. S6), the location of EBL seems to be the most significant difference between them.

Genetic Replacement of Arg and Cys in Region 6 Alters EBL Localization. To evaluate whether the Arg substitution at the second Cys position is responsible for the altered trafficking of *Py*EBL, we exchanged Cys and Arg in the 17X and 17XL lines by genetic modification (17X-CtoR and 17XL-RtoC). The parasites were also transfected with control constructs that do not alter the region 6 amino acid sequence (17X-CtoC and 17XL-RtoR) (Fig. 3*A*). Each of the transgenic parasites was evaluated for the correct integration of the constructs to the *pyebl* gene locus by specific PCR analysis followed by sequencing of the PCR-amplified products (not shown) and Southern blot analysis (Fig. 3*B*).

In the 17X line, replacement of Cys with Arg (17X-CtoR) altered the *Py*EBL localization from an apical pattern to a

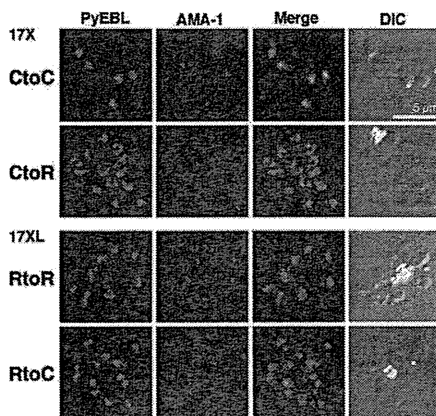

Fig. 4. Replacement of Cys to Arg in region 6 altered subcellular localization of *Py*EBL. Schizonts of transgenic parasite lines were incubated with mAb 5B10 (PyEBL), rabbit anti-AMA1 serum (AMA1), and DAPI (blue) for nuclear staining. DIC images are shown in the right-hand column. In the 17X background, control (CtoC) shows an apical *Py*EBL signal colocalized with AMA1, but replaced (CtoR) shows a 17XL pattern. Inversely, 17XL background control (RtoR) shows a diffused nonapical pattern, but replaced to cysteine (RtoC) shows an apical signal colocalized with AMA1.

nonapical diffused pattern, and *Py*EBL did not colocalize with AMA1. Furthermore, the replacement of Arg with Cys in the 17XL line (17XL-RtoC) altered the *Py*EBL localization from a nonapical diffused pattern to an apical pattern. Control parasites did not display altered *Py*EBL localization (Fig. 4). These results confirm that the observed substitution from Cys to Arg is responsible for the altered localization of *Py*EBL from micronemes to dense granules in the 17XL line.

EBL Localization Alters Erythrocyte-Type Preference and Course of Infection. To determine whether altered localization of *Py*EBL affects erythrocyte-type invasion preference, infected erythrocytes were examined by microscopy, and a selectivity index (SI) was obtained by calculating multiple parasite infection of single erythrocytes for each parasite line on postinfection day 3 in mice (13). We found that 17XL-RtoC predominantly invaded reticulocytes in the same way as the nonlethal 17X line. The SI of the 17XL line (2.38) was increased in 17XL-RtoC ($\approx$35; $P < 0.001$). On the other hand, 17X-CtoR was able to invade a variety of ages of erythrocytes, including mature erythrocytes, comparable to the lethal 17XL line, with the SI of the 17X line (16.78) reduced in 17X-CtoR ($\approx$4; $P < 0.001$; Table 1). These results demonstrate that the localization of *Py*EBL is responsible for the erythrocyte-type preference of the parasite.

Table 1. Selectivity index of WT and transgenic *Plasmodium yoelii* lines

Parasite	*n*	Selectivity index (range)
17X-CtoR 1	5	3.87 (1.86–5.32)
17X-CtoR 2	5	4.25 (2.38–7.97)
17X-CtoC	5	23.53 (16.49–36.00)
17X	5	16.78 (7.60–24.99)
17XL-RtoC 1	5	34.35 (29.18–38.05)
17XL-RtoC 2	5	35.99 (29.97–42.72)
17XL-RtoR	5	1.31 (0.57–2.13)
17XL	5	2.38 (1.58–3.75)

Selectivity indices were calculated from parasitized Giemsa-stained thin blood films collected from each infection.

Because erythrocyte-type preference frequently correlates with virulence in malaria parasites, we further analyzed the transgenic *P. yoelii* parasites for differences in the course of infection and survival of parasite-infected mice. Mice infected with the 17XL-RtoC line developed significantly lower parasitemias compared with the parental 17XL and control 17XL-RtoR lines (Fig. 5*A*), with 100% survival (Fig. 5*C*), whereas all mice infected with 17XL and 17XL-RtoR lines died by day 7 (Fig. 5*C*). The pattern observed for the 17XL-RtoC line was identical to that observed for the nonlethal 17X line. Thus, trafficking of *Py*EBL to the micronemes causes the virulence of the 17XL line to be reduced to the same level as the nonlethal 17X line, suggesting that *Py*EBL is a critical virulence determinant in the 17XL line. The parasitemia of mice infected with 17X-CtoR increased significantly compared with those infected with parental 17X and control 17X-CtoC lines during the acute phase of infection on days 4 to 5 ($P < 0.001$). However, the parasitemia did not reach the level observed for the lethal 17XL line, and it reduced to the same level observed for the 17X and 17X-CtoC lines by day 9 (Fig. 5*B*). No parasites were detectable by microscopy at day 17 (not shown). This suggests that the 17X-CtoR line is able to invade a greater repertoire of erythrocyte types than 17X but is unable to invade as many types as the 17XL line. This reduced capacity to invade multiple erythrocyte types compared with the 17XL line results in a nonlethal infection, in which all mice survive (Fig. 5*C*). Thus, displacement of the EBL from microneme was not sufficient to make this line fully lethal, suggesting the existence of other determinant(s).

Discussion

The results of this study indicate that replacement of Cys to Arg at the second Cys position of *Py*EBL region 6 is the major

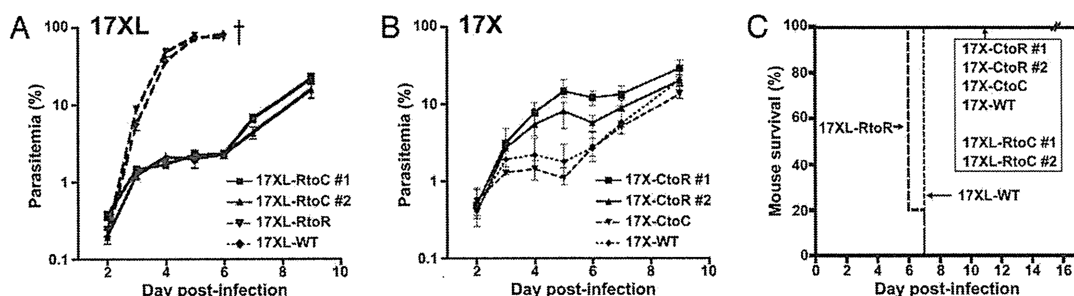

Fig. 5. Effect of the alteration of *pyebl* gene loci on the course of infection and parasite virulence in mice. Mice were i.v. inoculated with 1×10^6 parasitized erythrocytes from WT or transgenic parasite lines. (*A*) Parasitemia of 17XL-RtoC was dramatically reduced to the same level as that of the nonlethal 17X line. (*B*) Parasitemia of 17X-CtoR was significantly higher than parental 17X and control 17X-CtoC on days 4 and 5 ($P < 0.001$), the acute phase of infection; however, the pattern observed is intermediate between the lethal 17XL and nonlethal 17X lines. Parasitemias are plotted using the geometric mean and SD of log-transformed data from groups of 5 mice. (*C*) All mice infected with 17XL-RtoC survived, whereas all mice infected with parental 17XL and control 17XL-RtoR lines died by day 7. All mice infected with 17X, 17X-CtoC, and 17X-CtoR survived.

determinant of the difference between lethal and nonlethal lines of *P. y. yoelii* parasites. This substitution alters the intracellular organelle localization of *Py*EBL from the micronemes to the dense granules and alters the erythrocyte-type invasion preference, course of infection, and parasite virulence in the host.

The crystal structure of region 6 of *P. falciparum* EBA-175 indicates that the second Cys residue forms a disulfide bridge with the fourth Cys residue in this region. Arg substitution of the second Cys residue in the *P. yoelii* 17XL line abolishes this disulfide bridge and thus likely destroys the region 6 structure, which is critical for the trafficking of the protein to the micronemes. It is possible that an incorrectly folded region 6 would not allow the protein to be properly recognized by an (as yet uncharacterized) partner molecule responsible for the trafficking of the EBL protein to the micronemes (9). The mechanism involved in the trafficking of the mutated protein to the dense granules remains unresolved.

Using genetic modification, we have demonstrated that when *Py*EBL is trafficked to the microneme in the 17XL line genetic background, the erythrocyte-type invasion preference and the course of infection are comparable to those of the nonlethal 17X line. This indicates that the substitution of Cys to Arg is a major determinant of the lethal phenotype of the 17XL line. However, when *Py*EBL was not trafficked to the microneme in parasites with the 17X line genetic background, the course of infection was intermediate between the 2 parental lines, suggesting that although *Py*EBL is a critical determinant, other factor(s) are also involved in the lethal phenotype of the 17XL line. In *P. falciparum*, the expression of EBL seems to be co-operationally regulated with another *Plasmodium* ligand encoded by the *rbl* (*reticulocyte-binding-like*) multigene family that is composed of 6 members in *P. falciparum* and at least 14 members in *P. yoelii* (14–16); thus, the *P. yoelii rbl* protein, Py235, is a potential candidate for such factor(s). Consistent with this hypothesis is the finding that when Py235 expression was suppressed, the course of infection of the lethal *P. yoelii* YM line was altered from a lethal pattern to an intermediate pattern similar to that observed in the 17X-CtoR line shown in this study (17). On the basis of these observations, we propose that *Py*EBL may preferentially recognize reticulocytes and that the removal of *Py*EBL from the micronemes may result in free space within this organelle that may subsequently be filled with other ligand(s), possibly Py235, which consequently enables the parasite to invade a variety of erythrocyte types. Because different Py235 proteins may have different receptor specificities, parasite invasion preference and the subsequent course of infection may vary, depending on the Py235 member that fills the free space in the micronemes created by the absence of *Py*EBL. Such a switching mechanism for an erythrocyte invasion pathway has been previously proposed for *P. falciparum* (18).

A Linkage Group Selection analysis conducted by Pattaradilokrat et al. (19) identified a chromosomal region that included the *ebl* gene locus as a major determinant in the multiplication rate differences between the lethal *P. y. yoelii* YM line and a nonlethal 33X line, supporting the role of the EBL protein in controlling virulence phenotypes. Consistent with our findings that another genetic factor may be involved, they also identified a further genomic region on *P. yoelii* chromosome 5 or 6 that showed weak association with multiplication rate.

Because *Py*EBL localized in the dense granules is potentially nonfunctional, we attempted to disrupt the *pyebl* gene locus in both the 17X and 17XL lines (Fig. S7). However, repeated attempts failed to achieve this, despite the successful genomic integration of the control plasmid. This indicates that *Py*EBL is essential for parasite survival, even when it is not trafficked to the microneme. Two possible explanations for this may be that (*i*) an undetectable amount of *Py*EBL may still localize in the micronemes and remain functional, or (*ii*) *Py*EBL is functional during erythrocyte invasion (or for another unknown critical role during the life cycle), even when localized in the dense granules. Although a subgroup of the dense granules, known as exonemes, were recently reported to secrete their contents immediately before schizont rupture (20), we found that *Py*EBL was not detected on the surface of released individual merozoites of 17XL parasites (Fig. S8). Thus, the identity of the *Py*EBL-containing dense granules and the timing of *Py*EBL secretion from them, if at all, in the 17XL line remain undetermined.

In summary, we have found that a single nucleotide substitution altered the intracellular localization of the malaria parasite ligand *Py*EBL, which in turn altered erythrocyte invasion preference, course of infection, and parasite virulence. The virulence-mediating mechanism described in this report furthers our understanding of parasite–host interactions and has important implications for malaria vaccine design, especially those based on *Pv*DBP for *P. vivax* malaria.

Materials and Methods

Rodent Malaria Parasites. *Plasmodium yoelii* 17X, 17XL, and YM lines were maintained in BALB/c mice (Charles River Japan). The *P. yoelii* YM line was a kind gift from David Walliker of Edinburgh University.

DNA and RNA Isolation. Parasite genomic DNA (gDNA) was isolated from parasite-infected mouse blood using DNAzol BD reagent (Invitrogen). Parasite-infected blood was passed through a single CF11 cellulose column to remove leukocytes, and a schizont-enriched fraction was collected by differential centrifugation on a 50% Percoll solution (GE Healthcare). Total RNA was isolated from the schizont-enriched fraction using RNeasy Mini Kit (Qiagen). cDNA was synthesized using Omniscript reverse transcriptase (Qiagen) with random hexamer after DNase treatment.

PCR Amplification and Sequencing of *ebl* Genes. *ebl* genes were PCR-amplified from gDNA using KOD Plus DNA polymerase (Toyobo), with specific primers for each *ebl* gene designed using the *P. yoelii* genome database (The Institute for Genomic Research) and the *P. chabaudi* and *P. berghei* genome databases (The Sanger Centre). *ebl* sequences were determined by direct sequencing using an ABI PRISM 310 genetic analyzer (Applied Biosystems) from PCR-amplified products. Sequences were aligned using CLUSTALW implemented in MacVector (version 9.0; Accelrys).

Southern Blot Analysis. Five micrograms of *P. yoelii* gDNA were digested with EcoRI, EcoRV, ClaI, BanI, and NspI, and with BanI and HpaI with appropriate buffer, overnight. Digested gDNA was subjected to electrophoresis on 0.8% agarose gels, followed by alkaline transfer onto a Hybond-*n* + PVDF membrane (GE Healthcare). Probes were first PCR-amplified with 5′-TAAATCTAAATGGGATACAT-3′ and 5′-AGTTGGATTGATAGTTACAGATTC-3′ primers for the *pyebl* region, cloned into pGEM-T Easy plasmid (Promega), digested from the plasmid, and then hybridized onto membranes. Probes were labeled with the AlkPhos Direct kit (GE Healthcare), and a chemiluminescent signal developed with CDP-*star* reagent (GE Healthcare) was recorded on RX-U film (Fujifilm).

Recombinant Proteins. Expression plasmids were constructed on the basis of the pEU-E01-G(TEV)-N2 vector (21) by inserting PCR products amplified from *P. yoelii* 17X gDNA using KOD Plus DNA polymerase with the following primers: 5′-gagaCTCGAGGTTAATTTATTAAAAAGAACATATGAATCTTTCC-3′ and 5′-tctcGGATCC**CTA**TGAATAGCTCTCTTTTTGAAAAC-3′ for *Py*EBL regions 1 to 6 (R1–6; amino acid positions 28–787), 5′-gagaCTCGAGGTTAATTTATTAAAAAGAACATATGAATCTTTCC-3′ and 5′-tctcGGATCC**CTA**CAAATTATTATTAATAGGAGTATTACTGGG-3′ for regions 1 to 2 (R1–2; 28–436), 5′-gagaCTCGAGGAAAAAAATGGAAATGTAAATTACAAAG-3′ and 5′-tctcGGATCC**CTA**CAAATTATTATTAATAGGAGTATTACTGGG-3′ for region 2 (R2; 113–436), 5′-gagaCTCGAGTCTTCTGTTAAACCCAGTAATAC-3′ and 5′-tctcGGATCC**CTA**TACATTTTCGTTGGCTAGC-3′ for regions 3 to 5 (R3–5; 423–716), and 5′-gagagagaCTCGAGGACCCTAAACATGTATGTGTTGATAC-3′ and 5′-gagagagaGGATCC**TCA**TCCCATAAAGCTGGAAGAACTACAG-3′ for the 19-kDa region of the merozoite surface protein 1, *Py*MSP1 (*Py*MSP1–19; 1658–1757). The stop codon is shown in bold letters, and XhoI and BamHI restriction sites are underlined. GST-fused *Py*EBL or *Py*MSP1–19 recombinant proteins were expressed using the wheat germ cell-free protein synthesis system (Protemist DT; CellFree Sciences). Recombinant proteins were captured by a glutathione

column, washed, and eluted with glutathione elution buffer. Protein synthesis was confirmed by SDS-PAGE and Coomassie Brilliant Blue protein staining. Recombinant *Py*EBL R1–6 and R3–5 and *Py*MSP1–19 were used to produce antibodies, and *Py*EBL R1–2 and R2 were used for Western blot analysis.

Antibodies. To produce mouse anti-*Py*EBL and anti-*Py*MSP1 sera, female BALB/c mice were i.p. immunized 5 times with recombinant *Py*EBL R1–6 or 3 times with recombinant *Py*MSP1–19 emulsified with Freund's adjuvant, and killed for serum collection. To produce rabbit anti-*Py*EBL R3–5 serum, a female Japanese white rabbit was s.c. immunized 3 times with recombinant *Py*EBL R3–5 emulsified with Freund's adjuvant. To produce mouse anti-*Py*EBL monoclonal antibodies, the spleen was removed from a mouse immunized with recombinant *Py*EBL R1–6, and spleen cells were fused with a mouse myeloma cell line derived from a BALB/c mouse by the conventional polyethylene glycol method. Supernatants of cultured hybridoma colonies were tested with recombinant *Py*EBL R1–6 by ELISA and on *P. yoelii* 17X blood smears by indirect immunofluorescent assay. Positive hybridoma colonies were selected and cloned by 2 rounds of limiting dilution. The epitope region of each monoclonal antibody was tested by Western blot with a panel of recombinant *Py*EBL proteins. Anti-AMA1 rabbit serum was a gift from Carole Long of the National Institutes of Health.

Immunofluorescence Microscopy. *P. yoelii*–infected mouse erythrocytes were smeared onto glass slides, air dried, and stored at −80 °C without fixation. Slides were thawed, acetone-fixed, preincubated with PBS containing 5% nonfat milk at 37 °C for 30 min, incubated with mouse anti-*Py*EBL and rabbit anti-AMA1 sera at room temperature for 1 h, and then incubated with FITC-conjugated goat anti-(mouse IgG and IgM) antibody (Biosource International) and Alexa-546–conjugated goat antirabbit IgG antibody (Molecular Probes) at 37 °C for 30 min. Parasite nuclei were stained with DAPI. Differential interference contrast (DIC) and fluorescent images were obtained using a fluorescence microscope (BX50; Olympus) with a CCD digital camera (DC500; Leica) and processed using Adobe Photoshop CS (version 8.0; Adobe Systems).

Immunoelectron Microscopy. *P. yoelii*–infected mouse blood was fixed in 1% paraformaldehyde–0.1% glutaraldehyde in Hepes-buffered saline and embedded in LR white resin (Polysciences). Sections were blocked for 30 min in PBS–milk–Tween 20, incubated overnight at 4 °C in PBS–milk–Tween 20 containing mouse anti-*Py*EBL R1–6 serum, and then incubated for 1 h in PBS–milk–Tween 20 containing goat antimouse IgG conjugated with gold particles (10 nm diameter; Jansen). Sections were stained with 2% uranyl acetate in 50% methanol and examined by electron microscopy (JEM-1230; JEOL).

Genetic Modification of the *pyebl* Gene Locus. Two basic plasmids, pPbDT3U-B12 and pHDEF1-mh-R12, were constructed. A DNA fragment encoding cyan fluorescent protein was PCR-amplified from pECFP-C1 plasmid (Stratagene) using KOD Plus DNA polymerase with primers 5′-agcGCTAGCGTGAGCAAGGGCGAG-3′ (NheI site is underlined) and 5′-gacGTCGAC**GGATCC**TCTAGACTTGTACAGCTCGTCC-3′ (SalI and XbaI sites are underlined, and BamHI site is shown in bold) and ligated into the pGEM-T Easy plasmid. The insert was then digested with NheI and SalI, purified, and ligated into pRGDT-B12 (22) using the NheI and SalI sites, yielding pRCDT-B12. pRCDT-B12 was digested with ClaI and XbaI and filled with an oligonucleotide linker comprising cgatCTCGAG**CCCGGG**t and ctaga**CCCGGG**CTCGAGat to generate XhoI (underlined) and SmaI (bold) sites to yield pPbDT3U-B12. pHDEF1-mh (23) was digested with SmaI and ApaI to remove the 3′ untranslated region of histidine-rich protein 2, the ApaI cohesive end was blunted, and a Gateway gene conversion cassette C1 (Invitrogen) was inserted. The XhoI site was destroyed by XhoI digestion, filled in using KOD Plus DNA polymerase, and self-ligated to yield pHDEF1-mh-R12.

To modify the *pyebl* gene locus, a DNA fragment encoding *Py*EBL region 6 to the stop codon was PCR-amplified from gDNA of the *P. yoelii* 17XL line with primers 5′-gCCATGGGAACATAGAGACATTAAAAAAAGC-3′ and 5′-gCTCGAGATAAAAATCTACAGGTATATATTC-3′ (NcoI and XhoI sites are underlined) and cloned into pGEM-T Easy plasmids. The insert was ligated into the NcoI and XhoI sites of pPbDT3U-B12 to yield pR6Cyt-B12. DNA fragments encoding *Py*EBL region 3 to the stop codon were PCR-amplified from cDNA of the *P. yoelii* 17X and 17XL lines with primers 5′-atCTTCTGTTAAACCCAGTAATAC-3′ and 5′-ccAGATCTTTAATAAAAATCTACAGGTATATATTC-3′ (BglII site is underlined). PCR products were then ligated into the SmaI site of pR6Cyt-B12, yielding pR6Cyt+R3Cyt(X)-B12 and pR6Cyt+R3Cyt(XL)-B12, respectively. pR6Cyt+R3Cyt(X)-B12 and pR6Cyt+R3Cyt(XL)-B12 were subjected to a BP recombination reaction with the donor vector pDONR221 (Invitrogen) to produce the corresponding entry plasmids pENT.R6Cyt+R3Cyt(X) and pENT.R6Cyt+R3Cyt(XL). These entry plasmids were subjected to a LR recombination reaction (Invitrogen), according to the manufacturer's instructions, with pHDEF-1-mh-R12 to yield replacement constructs pYEBL-R6Cyt+R3Cyt(X) and pYEBL-R6Cyt+R3Cyt(XL), respectively.

P. yoelii schizont-enriched fraction was collected by differential centrifugation on 50% HistoDenz in PBS, and 20 μg of XhoI-digested transfection constructs were electroporated to 5×10^7 of enriched schizonts using the Nucleofector device (Amaxa) with human T cell solution under program U-33 (24). Transfected parasites were i.v. injected into 8-week-old BALB/c female mice, which were treated by i.p. injection with 1 mg/kg of pyrimethamine daily. Before inoculation of 17X line parasites, mice were treated with phenylhydrazine to increase the reticulocyte population in the blood. Drug-resistant parasites were cloned by limiting dilution. Integration of the transfection constructs was confirmed by PCR amplification with a unique set of primers for the modified *pyebl* gene locus, followed by sequencing and Southern blot analysis.

Course of Infection. To assess the course of infection of transgenic and WT parasite lines, 1×10^6 parasitized erythrocytes were injected i.v. into 8-week-old female BALB/c mice. Thin blood smears were made daily, stained with Giemsa's solution, and parasitemias were recorded. Mouse survival was evaluated by the Kaplan-Meier method. Parasitemias of each group were compared by 1-way ANOVA and Tukey's posttest, implemented in Prism 4.0 (GraphPad Software).

Selectivity Index. To compare erythrocyte preference between transgenic and WT *P. yoelii* parasite lines, a SI was calculated as follows: Multiple-infected erythrocytes divided by the expected number of multiple-infected erythrocytes, which was calculated from the number of infected erythrocytes and parasitemia (13). When the preferred erythrocyte type is limited, the observed number of multiple-infected erythrocytes increases. More than 200 parasitized erythrocytes were examined on Giemsa-stained thin blood smears collected on postinoculation day 3. The SI of each group was compared by 1-way ANOVA and Tukey's posttest, implemented in Prism 4.0.

For additional information see *SI Materials and Methods*.

ACKNOWLEDGMENTS. We thank D. Walliker for *P. yoelii* 33X, 33XPr3, and YM lines; C. Long for anti-AMA1 rabbit serum; H. A. del Portillo (Barcelona Centre for International Health Research, Barcelona) for pHDEF1-mh; Y. Tanaka, K. Kameda, and K. Oka (Integrated Center for Science, Ehime University) for their expertise; N. Kangwanrangsan (Ehime University, Matsuyama, Japan) for anti-*Py*MSP1–19 serum; and R. Culleton for critical reading. Preliminary sequence data for *P. berghei*, *P. chabaudi*, and *P. vinckei* were obtained from The Institute for Genomic Research. Animal experiments were carried out in compliance with the Guide for Animal Experimentation at Ehime University School of Medicine. This work was supported in part by Grants-in-Aids for Scientific Research 19790308 (to H.O.), 19590428 (to O.K.), 16390126 and 19390120 (to M. Torii), by Scientific Research on Priority Areas 19041053 (to T.T.) from the Ministry of Education, Culture, Sports, Science and Technology of Japan, and by Japan Society for the Promotion of Science–National University of Singapore Joint Research Program 07039011–000161 (to O.K.).

1. Landau I, Gautret P (1998), in *Malaria: Parasite Biology, Pathogenesis, and Protection*, ed Sherman IW (American Society for Microbiology, Washington, DC), pp 401–417.
2. Yoeli M, Hargreaves B, Carter R, Walliker D (1975) Sudden increase in virulence in a strain of *Plasmodium berghei yoelii*. *Ann Trop Med Parasitol* 69:173–178.
3. Playfair JH, De Souza JB, Cottrell BJ (1977) Protection of mice against malaria by a killed vaccine: Differences in effectiveness against *P. yoelii* and *P. berghei*. *Immunology* 33:507–515.
4. Miller LH, Mason SJ, Clyde DF, McGinniss MH (1976) The resistance factor to *Plasmodium vivax* in blacks. The Duffy-blood-group genotype, FyFy. *N Engl J Med* 295:302–304.
5. Wertheimer SP, Barnwell JW (1989) Plasmodium vivax interaction with the human Duffy blood group glycoprotein: Identification of a parasite receptor-like protein. *Exp Parasitol* 69:340–350.
6. Greenwood BM, et al. (2008) Malaria: Progress, perils, and prospects for eradication. *J Clin Invest* 118:1266–1276.
7. Adams JH, et al. (1992) A family of erythrocyte binding proteins of malaria parasites. *Proc Natl Acad Sci USA* 89:7085–7089.
8. Withers-Martinez C, et al. (2008) Malarial EBA-175 region VI crystallographic structure reveals a KIX-like binding interface. *J Mol Biol* 375:773–781.
9. Treeck M, et al. (2006) A conserved region in the EBL proteins is implicated in microneme targeting of the malaria parasite *Plasmodium falciparum*. *J Biol Chem* 281:31995–32003.

10. Sim BK, Toyoshima T, Haynes JD, Aikawa M (1992) Localization of the 175-kilodalton erythrocyte binding antigen in micronemes of *Plasmodium falciparum* merozoites. *Mol Biochem Parasitol* 51:157–159.
11. Adams JH, et al. (1990) The Duffy receptor family of *Plasmodium knowlesi* is located within the micronemes of invasive malaria merozoites. *Cell* 63:141–153.
12. Torii M, Adams JH, Miller LH, Aikawa M (1989) Release of merozoite dense granules during erythrocyte invasion by *Plasmodium knowlesi*. *Infect Immun* 57:3230–3233.
13. Simpson JA, Silamut K, Chotivanich K, Pukrittayakamee S, White NJ (1999) Red cell selectivity in malaria: A study of multiple-infected erythrocytes. *Trans R Soc Trop Med Hyg* 93:165–168.
14. Stubbs J, et al. (2005) Molecular mechanism for switching of *P. falciparum* invasion pathways into human erythrocytes. *Science* 309:1384–1387.
15. Iyer J, Grüner AC, Rénia L, Snounou G, Preiser PR (2007) Invasion of host cells by malaria parasites: A tale of two protein families. *Mol Microbiol* 65:231–249.
16. Carlton JM, et al. (2002) Genome sequence and comparative analysis of the model rodent malaria parasite *Plasmodium yoelii yoelii*. *Nature* 419:512–519.
17. Iyer JK, Amaladoss A, Ganesan S, Preiser PR (2007) Variable expression of the 235 kDa rhoptry protein of *Plasmodium yoelii* mediate host cell adaptation and immune evasion. *Mol Microbiol* 65:333–346.
18. Duraisingh MT, Maier AG, Triglia T, Cowman AF (2003) Erythrocyte-binding antigen 175 mediates invasion in *Plasmodium falciparum* utilizing sialic acid-dependent and -independent pathways. *Proc Natl Acad Sci USA* 100:4796–4801.
19. Pattaradilokrat S, Culleton RL, Cheesman SJ, Carter R (2009) Gene encoding erythrocyte binding ligand linked to blood stage multiplication rate phenotype in *Plasmodium yoelii yoelii*. *Proc Natl Acad Sci USA*, 10.1073/pnas.0811430106.
20. Yeoh S, et al. (2007) Subcellular discharge of a serine protease mediates release of invasive malaria parasites from host erythrocytes. *Cell* 131:1072–1083.
21. Tsuboi T, et al. (2008) Wheat germ cell-free system-based production of malaria proteins for discovery of novel vaccine candidates. *Infect Immun* 76:1702–1708.
22. Ghoneim A, Kaneko O, Tsuboi T, Torii M (2007) The *Plasmodium falciparum* RhopH2 promoter and first 24 amino acids are sufficient to target proteins to the rhoptries. *Parasitol Int* 56:31–43.
23. Fernandez-Becerra C, de Azevedo MF, Yamamoto MM, del Portillo HA (2003) Plasmodium falciparum: New vector with bi-directional promoter activity to stably express transgenes. *Exp Parasitol* 103:88–91.
24. Janse CJ, et al. (2006) High efficiency transfection of *Plasmodium berghei* facilitates novel selection procedures. *Mol Biochem Parasitol* 145:60–70.

Parasitology International 58 (2009) 243–248

Contents lists available at ScienceDirect

Parasitology International

journal homepage: www.elsevier.com/locate/parint

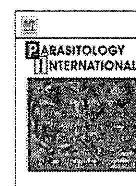

Enzymatic characterization of the *Plasmodium vivax* chitinase, a potential malaria transmission-blocking target

Satoru Takeo [a], Daisuke Hisamori [a], Shusaku Matsuda [a], Joseph Vinetz [b], Jetsumon Sattabongkot [c], Takafumi Tsuboi [a,d,*]

[a] Cell-Free Science and Technology Research Center, Ehime University, 3 Bunkyo-cho, Matsuyama, Ehime 790-8577, Japan
[b] Division of Infectious Diseases, University of California San Diego School of Medicine 9500 Gilman Drive, 0741 Palade Laboratories, La Jolla, CA 92093-0741, USA
[c] Department of Entomology, Armed Forces Research Institute of Medical Sciences, Bangkok 10400, Thailand
[d] Venture Business Laboratory, Ehime University, 3 Bunkyo-cho, Matsuyama, Ehime 790-8577, Japan

ARTICLE INFO

Article history:
Received 18 November 2008
Received in revised form 29 April 2009
Accepted 2 May 2009
Available online 8 May 2009

Keywords:
Chitinase
Transmission-blocking
Plasmodium vivax
Allosamidin

ABSTRACT

The chitinase (EC 3.2.1.14) of the human malaria parasite *Plasmodium falciparum*, PfCHT1, has been validated as a malaria transmission-blocking vaccine (TBV). The present study aimed to delineate functional characteristics of the *P. vivax* chitinase PvCHT1, whose primary structure differs from that of PfCHT1 by having proenzyme and chitin-binding domains. The recombinant protein rPvCHT1 expressed with a wheat germ cell-free system hydrolyzed 4-methylumbelliferone (4MU) derivatives of chitin oligosaccharides (β-1,4-poly-*N*-acetyl glucosamine (GlcNAc)). An anti-rPvCHT1 polyclonal antiserum reacted with *in vitro*-obtained *P. vivax* ookinetes in anterior cytoplasm, showing uneven patchy distribution. Enzymatic activity of rPvCHT1 shared the exclusive endochitinase property with parallelly expressed rPfCHT1 as demonstrated by a marked substrate preference for 4MU-GlcNAc$_3$ compared to shorter GlcNAc substrates. While rPvCHT1 was found to be sensitive to the general family-18 chitinase inhibitor, allosamidin, its pH (maximal in neutral environment) and temperature (max. at ~25 °C) activity profiles and sensitivity to allosamidin ($IC_{50} = 6$ μM) were different from rPfCHT1. The results in this first report of functional rPvCHT1 synthesis indicate that the *P. vivax* chitinase is enzymatically close to long form *Plasmodium* chitinases represented by *P. gallinaceum* PgCHT1.

© 2009 Elsevier Ireland Ltd. All rights reserved.

1. Introduction

To complete transmission between a vertebrate host and an anopheline mosquito, *Plasmodium* male and female gametes merge in the mosquito midgut to form zygotes that elongate into the invasive motile form, the ookinete. The ookinete must traverse the chitin-containing peritrophic matrix (PM) *en route* to invading the midgut epithelium to become a sporozoite-forming oocyst. The ookinete secretes a chitinase [1] that facilitates this process, as has been shown in gene knockout studies [2,3], membrane feeding assays with a chitinase inhibitor allosamidin [4], and with chitinase-specific antibodies [5,6]. Therefore, the chitinase is a potential target for transmission blocking of malaria with chemical or immunological strategies.

Genes encoding chitinases have been identified from several *Plasmodium* species, but functional analysis including studies on enzymatic activity has only been done with the chitinases PfCHT1 of *Plasmodium falciparum* [7] and PgCHT1 of *P. gallinaceum* [8]. *P. gallinaceum* is the only malaria parasite species in which more than one chitinase genes have been identified. Although both PgCHT1 [4,8] and PgCHT2 [5,8–10] are members of the family 18 chitinases, these enzymes differ significantly in their enzymatic properties including pH optima and quantitative sensitivity to allosamidin [8]. The short form PgCHT2 lacks two structure characteristics present in the long form PgCHT1; 1) a "repeat/insert" region to form a proenzyme domain, between N-terminal signal peptide and a catalytic domain, and 2) a putative chitin-binding domain at the C-terminus. The *P. falciparum* PfCHT1 and the chitinase of the chimpanzee malaria parasite *P. reichenowi* PrCHT1 are short forms; the enzymatic characteristics of PfCHT1 has been experimentally demonstrated to be more similar to the orthologous PgCHT2 than to PgCHT1 [7].

Detailed functional analysis including enzymatic characterization of PvCHT1, the chitinase of the other major human malaria parasite *P. vivax* is fundamental to assessing the potential of *Plasmodium* chitinase as a candidate transmission-blocking target. The deduced amino acid sequence from cloned *pvcht1* [11] indicates that this enzyme is orthologous to the long form of *Plasmodium* chitinase represented by PgCHT1. An unrooted phylogenetic tree of the conserved catalytic domain supports the clustering of PvCHT1 and PgCHT1 (TBLASTN amino acid identity values = 81%/positives = 92%) distant from another

* Corresponding author. Cell-Free Science and Technology Research Center, Ehime University, 3 Bunkyo-cho, Matsuyama, Ehime 790-8577, Japan. Tel.: +81 89 927 8277; fax: +81 89 927 9941.
E-mail address: tsuboi@ccr.ehime-u.ac.jp (T. Tsuboi).

1383-5769/$ – see front matter © 2009 Elsevier Ireland Ltd. All rights reserved.
doi:10.1016/j.parint.2009.05.002